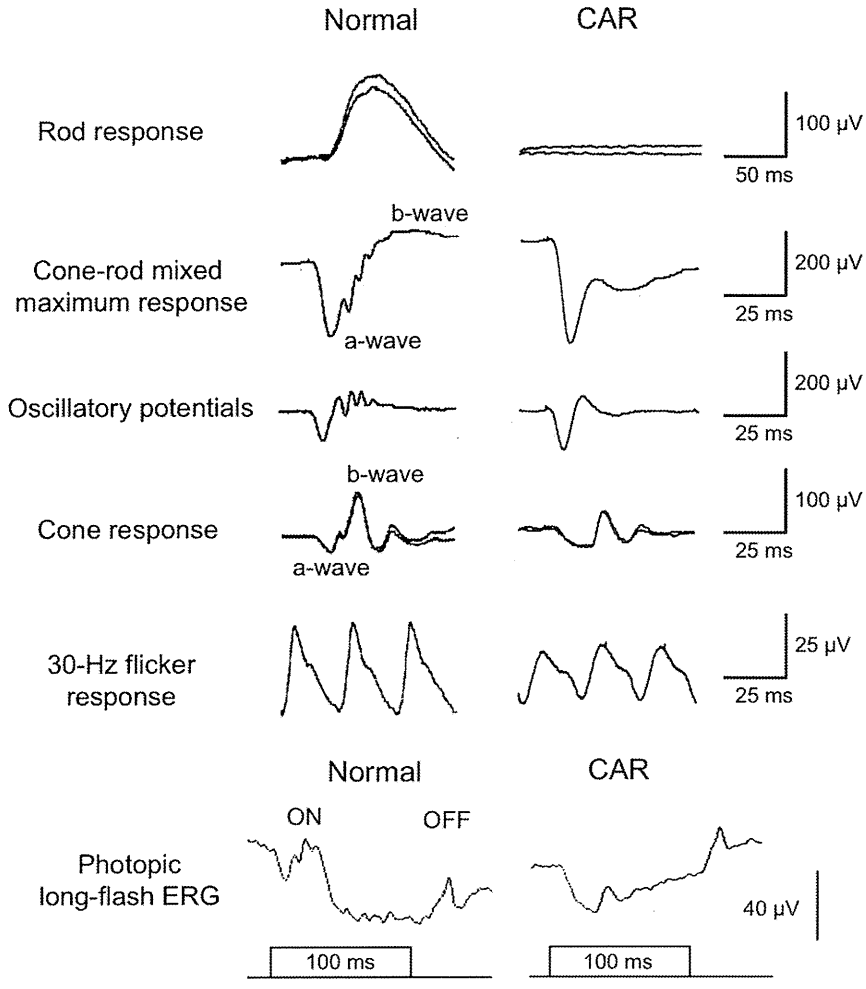

Figure 2. Full-field ERG recordings. The rod response was recorded with a blue light at an intensity of 5.2×10^{-3} cd-s/m^2 after 30 minutes of dark-adaptation. The cone-rod mixed maximum response was elicited by a white flash at an intensity of 44.2 cd-s/m^2. The oscillatory potentials were recorded with a white flash at an intensity of 44.2 cd-s/m^2 using a band-pass filter of 50–1000 Hz. The cone response and a 30 Hz flicker response were elicited by a white stimulus of 4 cd-s/m^2 and 0.9 cd-s/m^2, respectively, on a blue background of 30 cd/m^2. Photopic long-flash ERG responses were also elicited by long-duration flashes of 100 ms using a densely-packed array of white LEDs of 200 cd/m^2 on a white background of 30 cd/m^2.
doi:10.1371/journal.pone.0019911.g002

To examine whether the serum from the CAR patient recognized retinal bipolar cells, we carried out an immunohistochemical analysis on monkey and mouse retinas. We first performed immunohistochemistry on the retina of a 3-year-old rhesus monkey (*Macaca mulata*) and on the retina of a one-month-old C57/B6 mouse using the serum of the CAR patient, however, we did not obtain a significant staining signal above background (data not shown). We then concentrated the serum by IgG purification followed by filter spin column centrifugation and performed immunohistochemistry on the monkey retina using the concentrated serum (Fig. 3D–G). We observed a significant immunolabeling on the INL in the monkey retina (Fig. 3D, F) whereas the normal serum did not give a significant labeling (Fig. 3E, G). The antibodies immuolabeled both the bipolar side and amacrine side of the INL. Since most of the cells residing on the outer side of the INL are ON bipolar cells, at least some of the stained cells are ON bipolar cells. It should be noted some of the staining signals show a spotted pattern in the outer plexiform layer (Fig. 3F) as is observed in TRPM1 or mGluR6 immunostaining on the mouse retina [13], suggesting that the CAR patient serum recognizes the bipolar dendritic tips where some of the TRPM1 protein localizes.

Western blot analysis of the sera from MAR patients

Since the functional defect in the retina of MAR patients is known to be due to abnormal signal transmission between photoreceptors and ON bipolar cells [8,9], we then investigated whether or not autoantibodies to TRPM1 were also present in the sera of MAR patients. We obtained the sera of 26 MAR patients from two hospitals in Japan (Chiba University Hospital and Iwate Medical University Hospital) and Ocular Immunology Laboratory in the USA (Casey Eye Institute). We found that the sera from patients #8 and #23 exhibited a significant immunoreactive band against TRPM1-transfected cell lysates by Western blot analysis (Fig. 4A and B). The control serum showed no significant immune response against the TRPM1-transfected cell lysates (Fig. 3C). These results suggest that the sera from some MAR patients contain autoantibodies against TRPM1. Due to the limited volume of sera from the MAR patients, we could not try immunostaining on the monkey or the mouse retina using the serum from the patients #8 and #23.

MAR patient #8, was a 76-year-old man with a history of skin melanoma. He had ring scotomas and abnormal ERGs indicating that he had MAR. The other patient, MAR #23, was a 57-year-

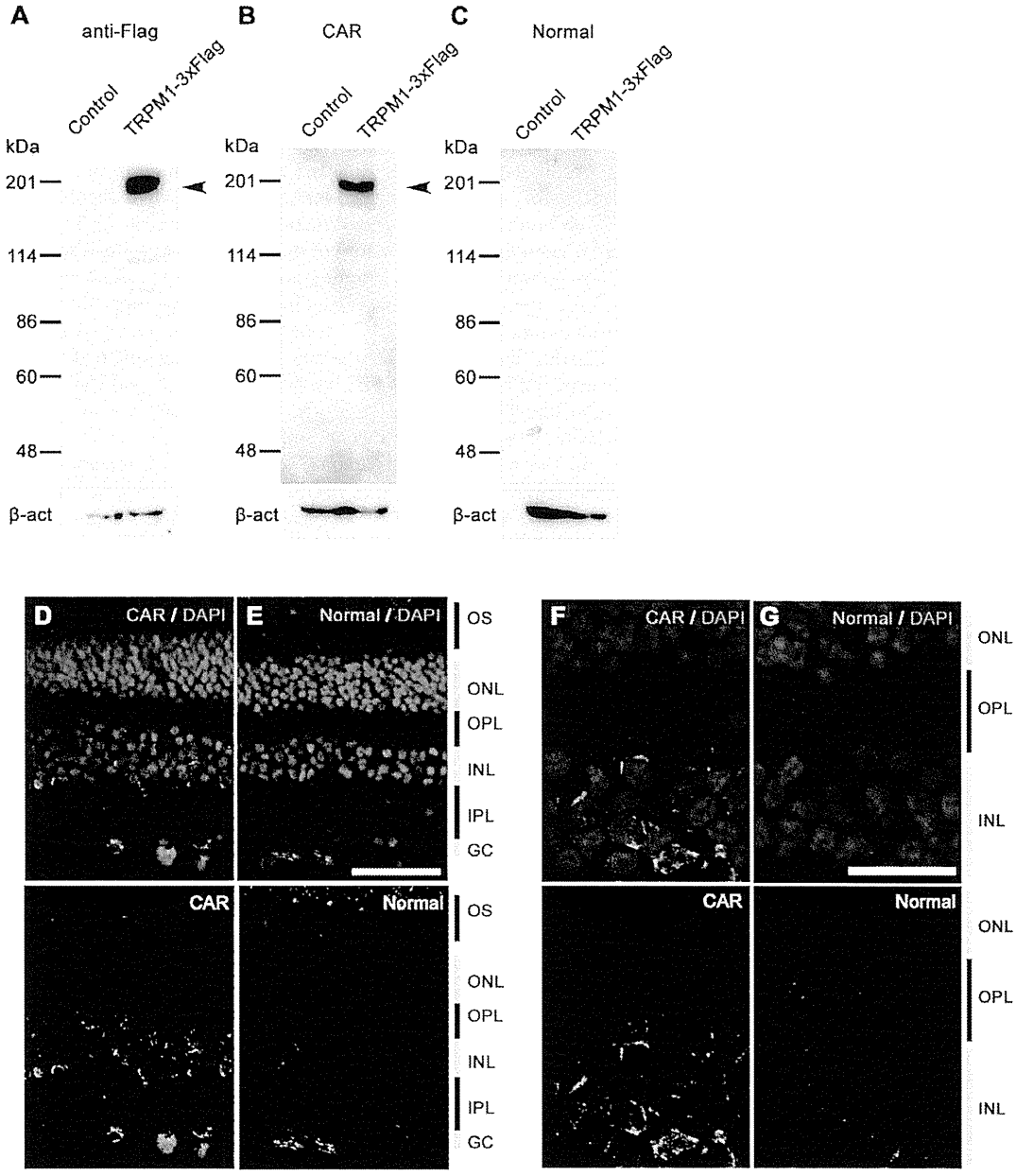

Figure 3. Immunostaining and Western blot analysis of human TRPM1 using serum from the CAR patient. (A–C) Immunoblots of the transfected cell lysates using an antibody against Flag tag (A), serum from CAR patient (B), and control serum (C). Arrowheads indicate the TRPM1-3xFlag protein bands. HEK293T cells were transfected with the pCAGGS or pCAGGS-human TRPM1-3xFlag plasmid, and cells were harvested after 48 hrs. β-actin (β-act) was used for a loading control. (D–G) Confocal images of a three-year-old rhesus monkey retina immunostained with the concentrated serum from the CAR patient (D, F) or the concentrated normal serum (E, G). Cell nuclei are visualized with DAPI. CAR patient serum presented signals on INL cells and the inner part of the OPL (D, F). Scale bar = 50 μm in (E) and 20 μm in (G).
doi:10.1371/journal.pone.0019911.g003

old man with poor night vision, abnormal scotopic ERGs and abnormal color vision. He had a history of skin melanoma and thyroid cancer. There was no other clinical information available on these two patients because these sera were obtained from other institutes several years before without detailed clinical information.

Discussion

PR, including MAR and CAR, presents visual disorders associated with systemic cancer. Antibodies against retinal cells and proteins have been detected in the sera of patients with PR suggesting an autoimmune basis for the etiology of the PR. The autoantibodies identified so far include rhodopsin, retinal transducin alpha and beta, recoverin, S-arrestin, α-enolase, carbonic anhydrase II, and heat shock protein-60 which reside abundantly in photoreceptors [1–10,16]. MAR and CAR can cause bipolar cell dysfunction [7–12]. The results of the ERG [8,9] and immunohistochemistry [7] studies suggested that the main target of MAR are retinal ON bipolar cells in both the rod and cone pathways. However, autoantibodies specifically reacting with a bipolar cell antigen had not been identified in the sera of patients with PR, including those with CAR and MAR. In the current study, we identified autoantibodies against TRPM1, a component of the ON bipolar cell transduction channel negatively regulated by Goα in the mGluR6 signaling pathway [13–15], in the

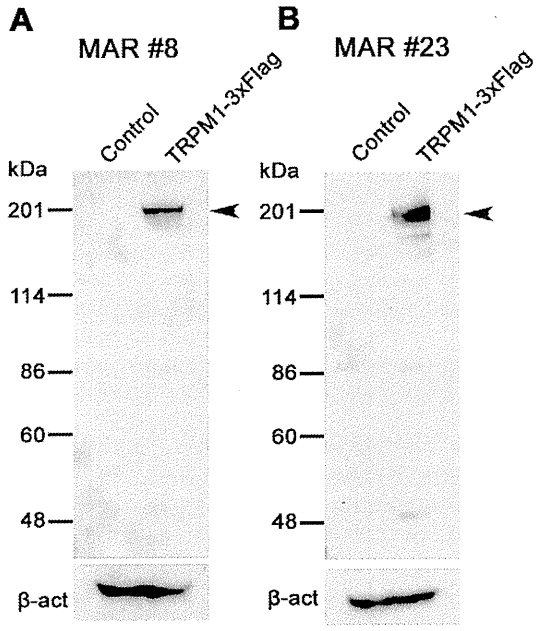

Figure 4. Western blot analysis of human TRPM1 using sera from the MAR patients. (A, B) Immunoblots of the transfected cell lysates using sera from MAR patient #8 (A) and MAR patient #23 (B). HEK293T cells were transfected with pCAGGS or pCAGGS-human TRPM1-3xFlag plasmid, and cells were harvested after 48 hrs. Arrowheads indicate the TRPM1-3xFlag protein bands. β-actin (β-act) was used for a loading control.
doi:10.1371/journal.pone.0019911.g004

sera of one CAR patient and two MAR patients. The CAR patient exhibited a dysfunction of ON bipolar cells, and to our knowledge, this is the first report on an autoantibody against a bipolar cell antigen in the serum of PR patients affecting the ON bipolar cell function.

Previously, we isolated a mouse *TRPM1-L* cDNA corresponding to the human long form of *TRPM1*, and found that the TRPM1-L protein is developmentally localized at the tips of the ON bipolar dendrites co-localizing with mGluR6, but not on OFF bipolar cells [13,14]. The *TRPM1* null mutant mouse completely loses the ON bipolar cell photoresponses to light, indicating that TRPM1 plays a critical role in the synaptic transmission from photoreceptors to ON-bipolar cells [13,15]. In addition, we demonstrated using a CHO cell reconstitution system that TRPM1-L is a nonselective cation channel which is negatively regulated by Goα downstream of the mGluR6 signaling cascade in ON bipolar cells [13]. Recently, four groups including ours independently reported that mutations of human *TRPM1* are associated with the complete-type of congenital stationary night blindness (cCSNB), an inherited human retinal disease [17–20]. cCSNB is a non-progressive retinal disease characterized by congenital night blindness with a moderate decrease in visual acuity and myopia [21-24]. Previous ERG studies have suggested that the defect in cCSNB patients lies in the signal transmission from photoreceptors to ON bipolar cells in both the rod and cone pathways [25–28]. We have identified five different mutations in our three cCSNB patients, and have shown that these mutations lead to either abnormal TRPM1 protein production or mislocalization of the TRPM1 protein in bipolar cell dendrites [17]. These results suggest that TRPM1 plays a critical role in mediating the photoresponses of ON bipolar cells in humans as well. Based on these findings, we hypothesize that the ectopic expression of TRPM1 in tumor cells of some CAR and MAR patients may result in aberrant production of autoantibodies to TRPM1 through B-lymphocytic responses [29–32]. These antibodies may react to the TRPM1 protein in retinal ON bipolar cells resulting in dysfunction of the TRPM1 transduction cation channel downstream of the mGluR6 signaling cascade. However, we could not confirm whether TRPM1 is expressed in the tumor cells of the three PR patients examined in this study [29] because tumor samples were not available.

Another question regarding the disease mechanism underlying PR is whether the binding of TRPM1 autoantibody to bipolar cells results in the cell death or dysfunction of bipolar cells. As far as we examined the retinal structure of the CAR patient using a spectral domain optical coherence tomography (SD-OCT) retinal imaging device, the structure of the retinal bipolar cell layer appeared to be well preserved even three months after the onset of symptoms (Fig.1D). This suggests that the autoantibodies reacting to TRPM1 cause dysfunction of the ON bipolar transduction pathway rather than bipolar cell death. However, further studies are needed to clarify the exact disease mechanism.

In the sera of MAR patients, several types of autoantibodies against retinal proteins have been reported, including the 22 kDa neuronal antigen GNB1, rhodopsin, S-arrestin, and aldolase-A and -C [10,16,33,34]. We initially considered that TRPM1 might be a major MAR target antigen, because TRPM1 is exclusively expressed in retinal ON bipolar cells. However, autoantibodies against TRPM1 were detected in only two out of 26 MAR. patients' sera (7.7%, Fig. 4A, B). We tested whether the sera of one CAR patient and 26 MAR patients recognized human mGluR6, which is specifically expressed in ON bipolar cells, however, none of the sera exhibited a significant band in Western blot analysis (data not shown). Thus, antigens other than TRPM1 or mGluR6 may be involved in the pathogenesis of a large proportion of MAR.

Immunohistochemical analyses using the serum of the CAR patient showed labeling in the inner nuclear layer and outer plexiform layer of the adult rhesus monkey retina (Fig. 3D–G), where the bipolar cell bodies and dendrites reside, respectively. This immunostaining pattern is somewhat similar to our previous immunostaining results on the mouse retina with specific antibody against mouse TRPM1-L, which corresponds to the human TRPM1 long form [13]. Other labeling was also observed in the amacrine cells and ganglion cells. The reason for the immunoreactivity with these cells is uncertain, however, it may be due to the presence of other autoantibodies against amacrine cell and ganglion cell antigens. Lu *et al.* reported the presence of various different autoantibodies in the serum of a single PR patient [10]. If this is the case, it may explain why our CAR patient displayed severely reduced visual sensitivities in the visual field tests (Fig. 1A) unlike cCSNB patients with TRPM1 mutations[17].

It should be noted that we did not confirm whether there are any antoantibodies against TRPM1 in the sera of normal subjects by using a large number of samples. However, this possibility is thought to be low, because Shimazaki *et al.* reported that the molecular weights of the IgGs with observed anti-retinal reactivity in 92 normal sera were smaller than 148 kDa, which is smaller than the TRPM1 molecular weight of ~200 kDa, although relatively high molecular weight reactivity was not intensively investigated [35].

One limitation of the current study is that we could not obtain detailed information on the two MAR patients, MAR #8 and #23, associated with the TRPM1 autoantibody. We confirmed that these two patients had skin melanomas accompanying the visual disturbances, but could not obtain a more detailed clinical history or data on visual acuity, visual field, or ERGs because these sera were sent from different hospitals several years ago. Thus, we do not know whether these two MAR patients really had retinal ON bipolar cell dysfunction. Further prospective studies of the TRPM1 autoantibodies in large numbers of MAR patients are needed.

In conclusion, our study suggests that TRPM1 may be one of the causative antigens responsible for PR associated with ON bipolar cell dysfunction.

Note added in proof

During the course of revision process of this manuscript, Dhingra *et al.* (J. Neurosci. 31, 3962–3967, 2011) independently reported the presence of autoantibodies against TRPM1 in two MAR patients. Our study reports on autoantibodies against TRPM1 in CAR serum in addition to MAR sera.

Materials and Methods

Subjects

The Nagoya University Hospital Ethics Review Board approved this study (approval ID 1131). Of the PR patients that were examined in the Nagoya University Hospital, one PR patient with lung cancer and ON bipolar cell dysfunction was studied in detail. The examinations included routine ophthalmological and electrophysiological tests. In addition, immunohistochemical and Western blot analyses were performed using the serum of this patient. The procedures used conformed to the tenets of the Declaration of Helsinki of the World Medical Association. A written informed consent was obtained from the patient after he was provided with sufficient information on the procedures to be used.

We also obtained sera of 26 patients with MAR from two hospitals in Japan (Chiba University Hospital and Iwate Medical University Hospital) and Ocular Immunology Laboratory in the USA (Casey Eye Institute) for Western blot analysis.

Ophthalmologic examinations

The ophthalmologic examination included best-corrected visual acuity, biomicroscopy, ophthalmoscopy, fundus photography, fluorescein angiography, static perimetry, and spectral-domain optical coherence tomography (SD-OCT). Static visual fields were obtained with the Humphrey 30-2 program (Carl Zeiss, Dublin, USA), and the results are shown in gray scale. SD-OCT was performed with a 9-mm horizontal scan through the midline with 50 averages (Spectralis HRA+OCT; Heidelberg Engineering, Vista, CA).

Electroretinograms (ERG)

Full-field ERGs were elicited with a Ganzfeld dome and recorded with a Burian-Allen bipolar contact lens electrode. The ground electrode was attached to the ipsilateral ear.

After 30 minutes of dark-adaptation, a rod response was elicited with a blue light at an intensity of 5.2×10^{-3} cd-s/m^2. A cone-rod mixed maximum response was elicited by a white flash at an intensity of 44.2 cd-s/m^2. A cone response and a 30 Hz flicker response were elicited by a white stimulus of 4 cd-s/m^2 and 0.9 cd-s/m^2, respectively, on a blue background of 30 cd/m^2. Full-field cone ERGs were also elicited by long-duration flashes of 100 ms using a densely packed array of white LEDs. The array was positioned at the top of the Ganzfeld dome and covered by a diffuser. The stimulus intensity and background illumination measured in the dome was 200 cd/m^2 and 30 cd/m^2, respectively. Responses were amplified by 10K and the band pass was set to 0.3 to 1000 Hz. The data were digitized at 4.3 kHz, and 5 to 20 responses were averaged (Neuropack, Nihonkohden, Tokyo, Japan).

Immunohistochemistry

For immunohistochemistry, patient and normal sera (300 µl) were purified using the Melon Gel IgG purification kit according to the manufacturer's protocol (Pierce Biotechnology, Rockford, IL) to remove IgM, and purified sera were concentrated by Amicon Ultra 100 (Millipore, MA). The rhesus monkey eye cup was fixed with 4% paraformaldehyde in PBS for 30 min at 4°C. The samples were cryoprotected with 30% sucrose in PBS and embedded in OCT compound (Sakura Finetechnical, Tokyo, Japan). These tissues were sliced with a Microm HM 560 cryostat microtome (Microm Laborgeräte GmbH, Walldorf, Germany) into 14 µm. Sections were washed twice in PBS for 5 min, permeabilized with 0.1% Triton-X100/PBS, then washed with PBS 3 times for 5 min, and incubated with PBS containing 4% donkey serum for 1 hr to block samples. For the immunoreaction, the samples were incubated with a purified normal or CAR serum (1:300) diluted in blocking buffer at 4°C overnight. After PBS-washing, these samples were incubated with a DyLight-488 conjugated donkey anti-human IgG (H+L) (1:400) as a secondary antibody (Jackson Immunoresearch Laboratories) at room temperature for 1 hr and washed with PBS.

Transfection and Western blot analyses

HEK293T cells were cultured in D-MEM containing 10% fetal bovine serum (FBS; Nissui, Tokyo, Japan). These cells were grown under 5% carbon dioxide at 37°C. The calcium phosphate method was used to transfect the cells. Transfected cells were incubated at 37°C for 48 hrs, and then harvested for further analysis. The proteins extracted from the cells were separated by SDS–PAGE on a 7.5% precast gel (ATTO, Tokyo, Japan), and then transferred to a polyvinylidene difluoride membrane using the Invitrogen iBlot system (Invitrogen, Carlsbad, CA, USA). The membrane was incubated with primary antibodies, mouse anti-Flag (1:1,000; Sigma, St Louis, MO), sera from patients (1:100), normal human serum (1:100), or mouse anti-β-actin (1:5,000; Sigma). The membrane was then incubated with a horseradish peroxidase-conjugated goat anti-mouse IgG (1:10,000; Zymed Laboratories, San Francisco, CA) or donkey anti-human IgG (1:10,000; Jackson Immuno Research Laboratories, West Grove, PA) as secondary antibodies. The bands were developed using Chemi-Lumi One L (Nacalai Tesque, Kyoto, Japan).

Acknowledgments

We thank Richard G. Weleber, Yozo Miyake, and Duco I. Hamasaki for helpful discussions of this study, Junko Hanaya for collecting the serum of our patients, and Mikiko Kadowaki, Aiko Ishimaru, Kaori Sone, and Shawna Kennedy for technical assistance.

Author Contributions

Conceived and designed the experiments: MK TF. Performed the experiments: MK RS SU YN NH. Analyzed the data: MK RS SU TF. Contributed reagents/materials/analysis tools: MK SU HO SY SM HT GA. Wrote the paper: MK TF. Supervised the project: MK HT TF.

References

1. Thirkill CE, FitzGerald P, Sergott RC, Roth AM, Tyler NK, et al. (1989) Cancer-associated retinopathy (CAR syndrome) with antibodies reacting with retinal, optic-nerve, and cancer cells. N Engl J Med 321: 1589–1594.
2. Chan JW (2003) Paraneoplastic retinopathies and optic neuropathies. Surv Ophthalmol 48: 12–38.
3. Heckenlively JR, Ferreyra HA (2008) Autoimmune retinopathy: A review and summary. Semin Immunopathol 30: 127–134.
4. Adamus G (2009) Autoantibody targets and their cancer relationship in the pathogenicity of paraneoplastic retinopathy. Autoimmun Rev 8: 410–414.

5. Thirkill CE, Roth AM, Keltner JL (1987) Cancer-associated retinopathy. Arch Ophthalmol 105: 372–375.
6. Jacobson DM, Thirkill CE, Tipping SJ (1990) A clinical triad to diagnose paraneoplastic retinopathy. Ann Neurol 28: 162–167.
7. Milam AH, Saari JC, Jacobson SG, Lubinski WP, Feun LG, et al. (1993) Autoantibodies against retinal bipolar cells in cutaneous melanoma-associated retinopathy. Invest Ophthalmol Vis Sci 34: 91–100.
8. Alexander KR, Fishman GA, Peachey NS, Marchese AL, Tso MOM (1992) "On" response defect in paraneoplastic night blindness with cutaneous malignant melanoma. Invest Ophthalmol Vis Sci 33: 477–483.
9. Lei B, Bush RA, Milam AH, Sieving PA (2000) Human melanoma-associated retinopathy (MAR) antibodies alter the retinal ON-response of the monkey ERG in vivo. Invest Ophthalmol Vis Sci 41: 262–266.
10. Lu Y, Jia L, He S, Hurley MC, Leys MJ, et al. (2009) Melanoma-associated retinopathy: a paraneoplastic autoimmune complication. Arch Ophthalmol 127: 1572–1580.
11. Jacobson DM, Adamus G (2001) Retinal anti-bipolar cell antibodies in a patient with paraneoplastic retinopathy and colon carcinoma. Am J Ophthalmol 131: 806–808.
12. Goetgebuer G, Kestelyn-Stevens AM, De Laey JJ, Kestelyn P, Leroy BP (2008) Cancer-associated retinopathy (CAR) with electronegative ERG: a case report. Doc Ophthalmol 116: 49–55.
13. Koike C, Obara T, Uriu Y, Numata T, Sanuki R, et al. (2010) TRPM1 is a component of the retinal ON bipolar cell transduction channel in the mGluR6 cascade. Proc Natl Acad Sci U S A 107: 332–337. Epub Dec. 4, 2009.
14. Koike C, Numata T, Ueda H, Mori Y, Furukawa T (2010) TRPM1: A vertebrate TRP channel responsible for retinal ON bipolar function. Cell Calcium 48: 95–101.
15. Morgans CW, Zhang J, Jeffrey BG, Nelson SM, Burke NS, et al. (2009) TRPM1 is required for the depolarizing light response in retinal ON-bipolar cells. Proc Natl Acad Sci U S A 106: 19174–19178.
16. Hartmann TB, Bazhin AV, Schadendorf D, Eichmüller SB (2005) SEREX identification of new tumor antigens linked to melanoma-associated retinopathy. Int J Cancer 114: 88–93.
17. Nakamura M, Sanuki R, Yasuma TR, Onishi A, Nishiguchi KM, et al. (2010) TRPM1 mutations are associated with the complete form of congenital stationary night blindness. Mol Vis 16: 425–437.
18. Li Z, Sergouniotis PI, Michaelides M, Mackay DS, Wright GA, et al. (2009) Recessive mutations of the gene TRPM1 abrogate ON bipolar cell function and cause complete congenital stationary night blindness in humans. Am J Hum Genet 85: 711–719.
19. van Genderen MM, Bijveld MM, Claassen YB, Florijn RJ, Pearring JN, et al. (2009) Mutations in TRPM1 are a common cause of complete congenital stationary night blindness. Am J Hum Genet 85: 730–736.
20. Audo I, Kohl S, Leroy BP, Munier FL, Guillonneau X, et al. (2009) TRPM1 is mutated in patients with autosomal-recessive complete congenital stationary night blindness. Am J Hum Genet 85: 720–729.
21. Miyake Y, Yagasaki K, Horiguchi M, Kawase Y, Kanda T (1986) Congenital stationary night blindness with negative electroretinogram: A new classification. Arch Ophthalmol 104: 1013–1020.
22. Bech-Hansen NT, Naylor MJ, Maybaum TA, Sparkes RL, Koop B, et al. (2000) Mutations in NYX, encoding the leucine-rich proteoglycan nyctalopin, cause X-linked complete congenital stationary night blindness. Nat Genet 26: 319–23.
23. Pusch CM, Zeitz C, Brandau O, Pesch K, Achatz H, et al. (2000) The complete form of X-linked congenital stationary night blindness is caused by mutations in a gene encoding a leucine-rich repeat protein. Nat Genet 26: 324–327.
24. Dryja TP, McGee TL, Berson EL, Fishman GA, Sandberg MA, et al. (2005) Night blindness and abnormal cone electroretinogram ON responses in patients with mutations in the GRM6 gene encoding mGluR6. Proc Natl Acad Sci USA 102: 4884–4889.
25. Miyake Y, Yagasaki K, Horiguchi M, Kawase Y (1987) On- and off-responses in photopic electroretinogram in complete and incomplete types of congenital stationary night blindness. Jpn J Ophthalmol 31: 81–87.
26. Houchin K, Purple RL, Wirtschafter JD (1991) X-linked congenital stationary night blindness and depolarizing bipolar system dysfunction. [ARVO abstract]. Invest Ophthalml Vis Sci 32: S1229.
27. Young RSL (1991) Low-frequency component of the photopic ERG in patients with X-linked congenital stationary night blindness. Clin Vis Sci 6: 309–315.
28. Khan NW, Kondo M, Hiriyanna KT, Jamison JA, Bush RA, et al. (2005) Primate retinal signaling pathways: Suppressing ON-pathway activity in monkey with glutamate analogues mimics human CSNB1-NYX genetic night blindness. J Neurophysiol 93: 481–492.
29. Polans AS, Witkowska D, Haley TL, Amundson D, Baizer L, et al. (1995) Recoverin, a photoreceptor-specific calcium-binding protein, is expressed by the tumor of a patient with cancer-associated retinopathy. Proc Natl Acad Sci U S A 92: 9176–9180.
30. Matsubara S, Yamaji Y, Sato M, Fujita J, Takahara J (1996) Expression of a photoreceptor protein, recoverin, as a cancer-associated retinopathy autoantigen in human lung cancer cell lines. Br J Cancer 74: 1419–1422.
31. Ohguro H, Odagiri H, Miyagawa Y, Ohguro I, Sasaki M, et al. (2004) Clinicopathological features of gastric cancer cases and aberrantly expressed recoverin. Tohoku J Exp Med 202: 213–219.
32. Bazhin AV, Schadendorf D, Willner N, De Smet C, Heinzelmann A, et al. (2007) Photoreceptor proteins as cancer-retina antigens. Int J Cancer 120: 1268–76.
33. Keltner JL, Thirkill CE (1999) The 22-kDa antigen in optic nerve and retinal diseases. J Neuroophthalmol 19: 71–83.
34. Potter MJ, Adamus G, Szabo SM, Lee R, Mohaseb K, et al. (2002) Autoantibodies to transducin in a patient with melanoma-associated retinopathy. Am J Ophthalmol 134: 128–30.
35. Shimazaki K, Jirawuthiworavong GV, Heckenlively JR, Gordon LK (2008) Frequency of anti-retinal antibodies in normal human serum. J Neuro-Ophthalmol 28: 5–11.

miR-124a is required for hippocampal axogenesis and retinal cone survival through Lhx2 suppression

Rikako Sanuki[1,2], Akishi Onishi[1,2], Chieko Koike[1], Rieko Muramatsu[3], Satoshi Watanabe[1,2], Yuki Muranishi[1], Shoichi Irie[1,2], Shinji Uneo[4], Toshiyuki Koyasu[4], Ryosuke Matsui[5], Yoan Chérasse[6], Yoshihiro Urade[6], Dai Watanabe[5], Mineo Kondo[4], Toshihide Yamashita[3] & Takahisa Furukawa[1,2]

MicroRNA-124a (miR-124a) is the most abundant microRNA expressed in the vertebrate CNS. Despite past investigations into the role of miR-124a, inconsistent results have left the *in vivo* function of miR-124a unclear. We examined the *in vivo* function of miR-124a by targeted disruption of *Rncr3* (*retinal non-coding RNA 3*), the dominant source of miR-124a. *Rncr3*$^{-/-}$ mice exhibited abnormalities in the CNS, including small brain size, axonal mis-sprouting of dentate gyrus granule cells and retinal cone cell death. We found that *Lhx2* is an *in vivo* target mRNA of miR-124a. We also observed that LHX2 downregulation by miR-124a is required for the prevention of apoptosis in the developing retina and proper axonal development of hippocampal neurons. These results suggest that miR-124a is essential for the maturation and survival of dentate gyrus neurons and retinal cones, as it represses *Lhx2* translation.

MicroRNAs (miRNAs) are small RNAs that regulate gene expression by base-pairing to mRNAs. Notably, miR-124a is completely conserved at the nucleotide level from worms to humans and is estimated to be the most abundant miRNA in the brain, accounting for 25–48% of all brain miRNAs[1]. In addition, the human miR-124a-1 locus is located in the chromosome 8p23 region, which is rich in genes that have been implicated in neuropsychiatric disorders, microcephaly and epilepsy[2]. Overexpression of miR-124a in HeLa cells leads to the suppression of a large number of non-neuronal transcripts[3]. Moreover, a neurogenesis suppressor gene, *Ctdsp1*, and a neuron-specific splicing repressor gene, *Ptbp1*, have been identified as miR-124a target genes *in vitro*[4,5], and an increase of *Ptbp1* mRNA was observed in the telencephalon of a *Dicer* conditional knockout mouse[5]. *In vivo* knockdown of miR-124a in mouse SVZ cells identified *Sox9*, a neurogenesis suppressor gene, as a miR-124a target, suggesting that miR-124a controls neurogenesis through suppression of *Sox9* translation[6]. One study found that miR-124a is required for neuronal determination in the developing chick neural tube[4]. On the other hand, another study reported that miR-124a is not involved in the initial neuronal differentiation in the developing chick spinal cord[7]. A *Dicer* conditional knockout mice exhibited initial neurogenesis in the absence of miRNA production[8,9]. Considering these inconsistent observations, the target genes of miR-124a and its functional role in neural differentiation remain ambiguous.

RESULTS

Rncr3 is the dominant source of miR-124a

Previously, we used a screen to identify functionally important molecules in the retina[10] and isolated mouse *Rncr3* cDNA[11], which is highly expressed in the retina. We examined the expression profiles of *Rncr3* by northern blot analysis and detected a ~4.1-kb full-length *Rncr3* band specifically in the CNS tissues (**Fig. 1a**). We identified a stem loop of precursor miR-124a-1 (pre-miR-124a-1), which is encoded in exon of *Rncr3*. *Rncr3* fulfilled certain criteria for being a miR-124a precursor, including high expression in the brain, nuclear localization and the presence of a consensus sequence[12] (data not shown). We examined the expression patterns of *pre-miR-124a* and *miR-124a* and confirmed that they were specifically expressed in the CNS, including the retina (**Fig. 1b**). We then investigated the localization of *Rncr3* and miR-124a in the developing retina and brain using *in situ* hybridization (**Fig. 1c–i**). Both *Rncr3* and miR-124a signals were strongly detected in ganglion cells and differentiating neurons at embryonic day 13.5 (E13.5; **Fig. 1c,f**), and those signals gradually increased until the mice were 1 month old (**Fig. 1d,e,g,h**). The abundant miR-124a signals in photoreceptor cells accumulated in the inner segment from postnatal day 1 (P1) to adulthood (1 month of age; **Fig. 1g,h**). In the adult mice, the miR-124a signal was detected in differentiated neurons, except for putative Müller glial cells in the inner nuclear layer (**Fig. 1e,h**), consistent with previous findings[13]. In the P6 brain, *Rncr3* RNA was broadly expressed, especially in the hippocampus and the upper third of the cortex (**Fig. 1i**). These results suggest that *Rncr3* is specifically expressed in the CNS and functions as a primary miR-124a-1 (pri-miR-124a-1).

To determine the function of miR-124a *in vivo*, we generated *Rncr3*$^{-/-}$ mice by replacing all of the exons of *Rncr3* with the *PGK-neo* cassette (**Fig. 2a–c**). *Rncr3*$^{-/-}$ mice were initially viable and appeared to be normal; however, about two-thirds of the *Rncr3*$^{-/-}$ mice gradually

[1]Department of Developmental Biology, Osaka Bioscience Institute, Suita, Osaka, Japan. [2]Japan Science and Technology Agency (JST), Core Research for Evolutional Science and Technology (CREST), Osaka Bioscience Institute, Suita, Osaka, Japan. [3]Department of Molecular Neuroscience, Graduate School of Medicine, Osaka University, Suita, Osaka, Japan. [4]Department of Ophthalmology, Nagoya University Graduate School of Medicine, Showa-ku, Nagoya, Japan. [5]Department of Biological Sciences, Faculty of Medicine, Graduate School of Biostudies, Kyoto University, Yoshida, Sakyo-ku, Kyoto, Japan. [6]Department of Molecular Behavioral Biology, Osaka Bioscience Institute, Suita, Osaka, Japan. Correspondence should be addressed to T.F. (furukawa@obi.or.jp).

Received 2 May; accepted 30 June; published online 21 August 2011; doi:10.1038/nn.2897

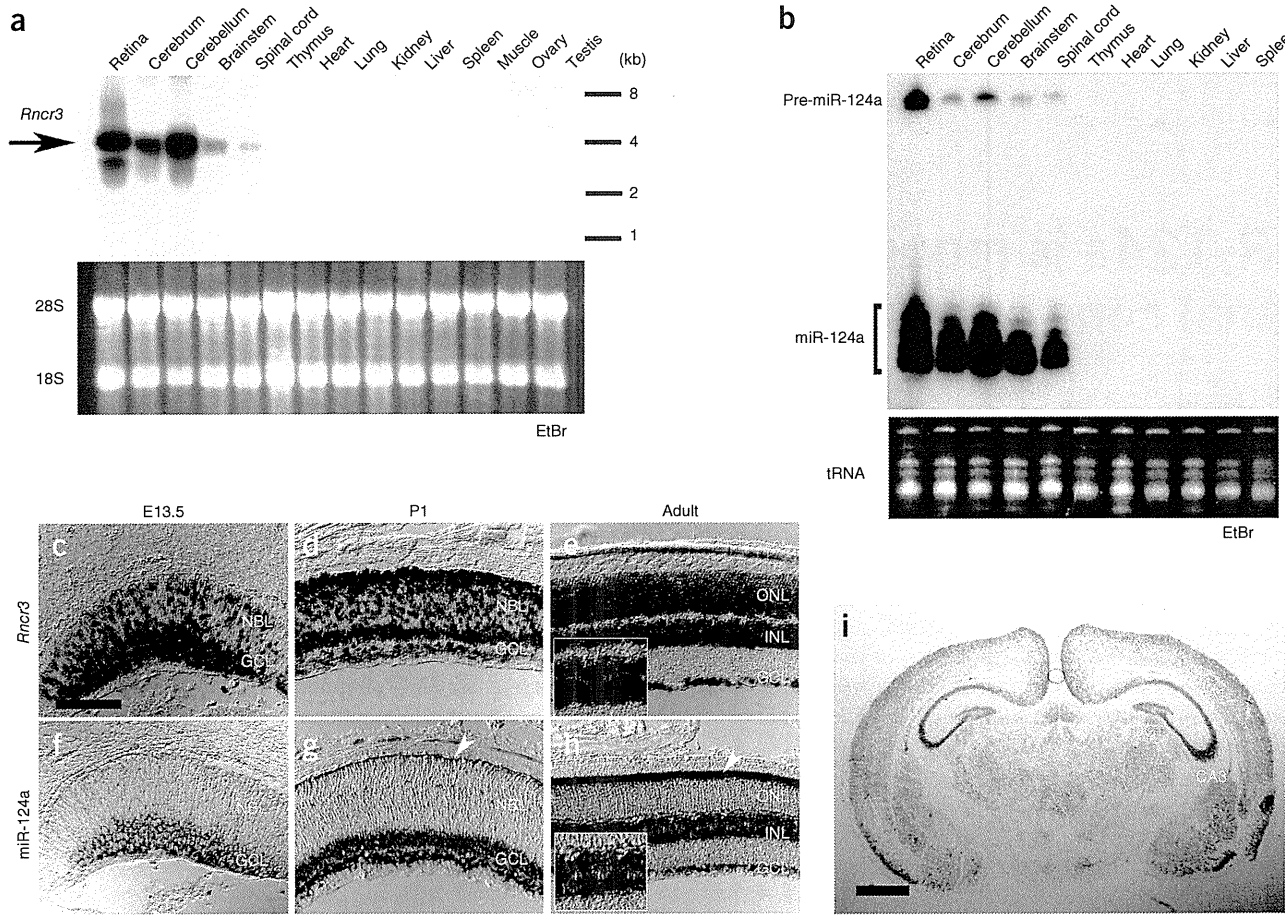

Figure 1 Expression of *Rncr3* and miR-124a. (**a**) Northern blot analysis of *Rncr3* transcripts in adult mouse tissues. The arrow indicates the approximately 4.1-kb *Rncr3* full-length mRNA. The lower panel shows ethidium bromide (EtBr) staining of RNA. (**b**) Northern blot analysis of miR-124a in adult mouse tissues. The upper panel shows miR-124a signals obtained from LNA-modified anti–miR-124a probe. The lower panel shows EtBr staining of small RNA. (**c**–**h**) Expression of *Rncr3* (**c**–**e**) and miR-124a (**f**–**h**) was detected by *in situ* hybridization in the developing retina at E13.5 (**c**,**f**), P1 (**d**,**g**) and in adult mice (1 month old, **e**,**h**). miR-124a signal was detected in the developing photoreceptor layer at P1 and the inner segments of photoreceptors in adults (**g** and **h**, arrowheads). The small boxes in **e** and **h** show unstained blank spots by *in situ* hybridization, which may correspond to Müller glia cells in the inner nuclear layer (INL). Scale bar represents 100 μm. (**i**) Expression of *Rncr3* in the developing brain at P6. Scale bar represents 1 mm. CTX, cortex; DG, dentate gyrus; GCL, ganglion cell layer; NBL, neuroblastic layer; ONL, outer nuclear layer.

became debilitated and died around P20 for unknown reasons. We compared miR-124a expression among wild-type, $Rncr3^{+/-}$ and $Rncr3^{-/-}$ mice and found that miR-124a band intensities were substantially reduced by 60–80% in all of the $Rncr3^{-/-}$ CNS regions that we examined at P14 (**Fig. 2d**). We then performed northern blots for miR-124a and an absolute quantitative RT-PCR (qPCR) assay for pri-miR-124a-1, pri-miR-124a-2 and pri-miR-124a-3 using the retina, hippocampus and cortex of P6 wild-type and $Rncr3^{-/-}$ mice (**Supplementary Fig. 1**). miR-124a expression was reduced by 60–80% in $Rncr3^{-/-}$ mice (**Supplementary Fig. 1a**) and pri-miR-124a-3 was undetectable in both wild-type and $Rncr3^{-/-}$ mice (**Supplementary Fig. 1b**), indicating that *Rncr3* (pri-miR-124a-1) is the dominant source of miR-124a.

We then examined the tissue distribution of miR-124a in developing $Rncr3^{-/-}$ mice using *in situ* hybridization to identify tissues in which miR-124a knockout was not compensated for by expression of pre-miR-124a-2 or pre-miR-124a-3. miR-124a expression was substantially reduced and barely detectable in the presumptive photoreceptor layer (PPL), where cone photoreceptor neurogenesis occurs from E11 to E18 (refs. 14,15), of $Rncr3^{-/-}$ retina at E15.5 (**Fig. 2e–h**), whereas NEUROD1, a neuronal differentiation and early photoreceptor marker, was detected at normal levels (wild type, 908.5 ± 58.2 cells per section; $Rncr3^{-/-}$, 919 ± 33.8; $P = 0.79$; **Fig. 2i–l**). In the E17.5 wild-type retina, pri-miR-124a-1 (*Rncr3*) was strongly observed in the PPL; however, the pri-miR-124a-2 host gene was barely expressed and pri-miR-124a-3 was undetectable (**Supplementary Fig. 2a–f**), suggesting that pri-miR124a-1 is the predominant source of miR-124a in the PPL.

We next observed sections of the P6 developing $Rncr3^{-/-}$ brain (**Fig. 2m–p**). The $Rncr3^{-/-}$ brain was smaller than that of the wild type, but its morphology was not substantially affected (**Fig. 2m,n**). miR-124a expression was significantly reduced in the $Rncr3^{-/-}$ brain compared with that in the wild-type brain, as determined by *in situ* hybridization (**Fig. 2o,p**). We found an especially substantial loss of miR-124a expression in the $Rncr3^{-/-}$ hippocampal dentate gyrus (**Fig. 2p**). Our results suggest that miR-124a expression is almost abolished in the developing cone photoreceptor layer and dentate gyrus in the hippocampus. Thus, we focused our analysis on retinal cone photoreceptors and the dentate gyrus.

Rncr3$^{-/-}$ mice exhibit neuronal dysfunction and dysmaturation

We first analyzed cone cells in the $Rncr3^{-/-}$ retina. We performed flat-mount immunostaining using 2-month-old $Rncr3^{-/-}$ retinas and

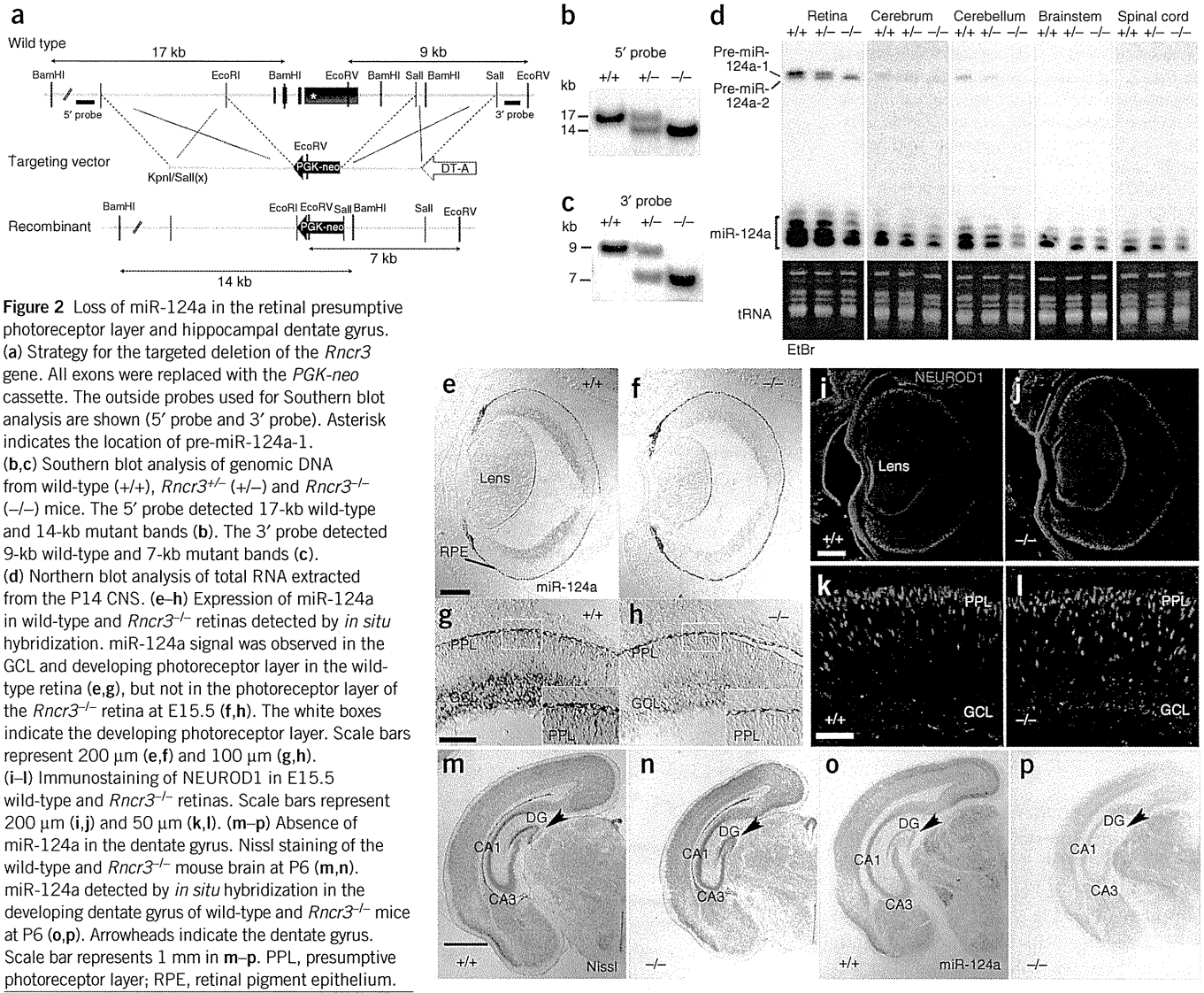

Figure 2 Loss of miR-124a in the retinal presumptive photoreceptor layer and hippocampal dentate gyrus. (**a**) Strategy for the targeted deletion of the *Rncr3* gene. All exons were replaced with the *PGK-neo* cassette. The outside probes used for Southern blot analysis are shown (5′ probe and 3′ probe). Asterisk indicates the location of pre-miR-124a-1. (**b**,**c**) Southern blot analysis of genomic DNA from wild-type (+/+), *Rncr3*$^{+/-}$ (+/–) and *Rncr3*$^{-/-}$ (–/–) mice. The 5′ probe detected 17-kb wild-type and 14-kb mutant bands (**b**). The 3′ probe detected 9-kb wild-type and 7-kb mutant bands (**c**). (**d**) Northern blot analysis of total RNA extracted from the P14 CNS. (**e**–**h**) Expression of miR-124a in wild-type and *Rncr3*$^{-/-}$ retinas detected by *in situ* hybridization. miR-124a signal was observed in the GCL and developing photoreceptor layer in the wild-type retina (**e**,**g**), but not in the photoreceptor layer of the *Rncr3*$^{-/-}$ retina at E15.5 (**f**,**h**). The white boxes indicate the developing photoreceptor layer. Scale bars represent 200 μm (**e**,**f**) and 100 μm (**g**,**h**). (**i**–**l**) Immunostaining of NEUROD1 in E15.5 wild-type and *Rncr3*$^{-/-}$ retinas. Scale bars represent 200 μm (**i**,**j**) and 50 μm (**k**,**l**). (**m**–**p**) Absence of miR-124a in the dentate gyrus. Nissl staining of the wild-type and *Rncr3*$^{-/-}$ mouse brain at P6 (**m**,**n**). miR-124a detected by *in situ* hybridization in the developing dentate gyrus of wild-type and *Rncr3*$^{-/-}$ mice at P6 (**o**,**p**). Arrowheads indicate the dentate gyrus. Scale bar represents 1 mm in **m**–**p**. PPL, presumptive photoreceptor layer; RPE, retinal pigment epithelium.

observed a significant reduction of the cone cell number and of mRNA expression of cone-specific genes ($P < 0.001$; **Fig. 3a–d**). To evaluate the physiological function of the *Rncr3*$^{-/-}$ retina *in vivo*, we recorded scotopic and photopic electroretinograms (ERGs) from 2-month-old wild-type and *Rncr3*$^{-/-}$ mice. Both the waveforms and amplitudes of a- and b-waves of scotopic ERGs were very similar between wild-type and *Rncr3*$^{-/-}$ mice (**Fig. 3e–g**). In contrast, the amplitudes of the photopic ERGs of *Rncr3*$^{-/-}$ mice were significantly smaller than those of wild-type mice at all stimulus intensities ($P < 0.05$; **Fig. 3h–j**). The amplitudes of the a-waves, which originate from cone photoreceptors, were less than one-third of those of wild-type mice. Moreover, we found that some opsin-positive cone cells were ectopically localized in the *Rncr3*$^{-/-}$ retina (**Supplementary Fig. 3a–g**). We also examined the development of other retinal cell types in 2-month-old *Rncr3*$^{-/-}$ mouse retinas by immunostaining (**Supplementary Fig. 4a–g**). Rod photoreceptor cells, bipolar cells, amacrine cells, horizontal cells, ganglion cells and Müller glial cells were unaffected. These results indicate that cone photoreceptors are impaired in *Rncr3*$^{-/-}$ mice.

In the developing mouse retina, the expression of TRβ2, an early cone marker, peaks at E17.5 (ref. 16). We examined the number of TRβ2-positive cells in the *Rncr3*$^{-/-}$ retina (**Supplementary Fig. 5a–c**). The number of cones was unaltered in the *Rncr3*$^{-/-}$ retina at E17.5 (**Supplementary Fig. 5c**). Notably, we found some mis-localized TRβ2-positive cells in the E17.5 mutant retina (**Supplementary Fig. 5b**). We then examined the expression of *Crx* and *Otx2*, photoreceptor cell differentiation genes[17–19], and *Neurogenin 2* (*Ngn2*, also known as *Neurog2*), a proneural gene, in both the wild-type and *Rncr3*$^{-/-}$ retinas at E13.5 by *in situ* hybridization and qPCR analysis (**Supplementary Fig. 5d–n**). In contrast with our cone number results, we found no apparent effect on early neurogenesis by quantitatively measuring *Neurod1*, *Trβ2*, *Crx*, *Otx2* and *Ngn2* in wild-type and *Rncr3*$^{-/-}$ retinas, although miR-124a expression was reduced (**Figs. 2i–m** and **3a–d** and **Supplementary Fig. 5a–n**). We examined apoptosis by TUNEL assay in wild-type and *Rncr3*$^{-/-}$ retinas, and found that the number of TUNEL-positive cells was significantly increased in the P3 *Rncr3*$^{-/-}$ retina ($P < 0.05$; **Supplementary Fig. 6a–c**). We further observed an increase in the number of TRβ2 and active caspase-3 double-positive cells and a decrease in the number of TRβ2-positive, caspase-3–negative cells in the *Rncr3*$^{-/-}$ retina (**Fig. 3k–p**), suggesting that the number of cone cells was reduced by apoptosis after neurogenesis. Furthermore, a recent study found that miR-124a was substantially reduced in anaplastic astrocytomas[20]. Thus, we

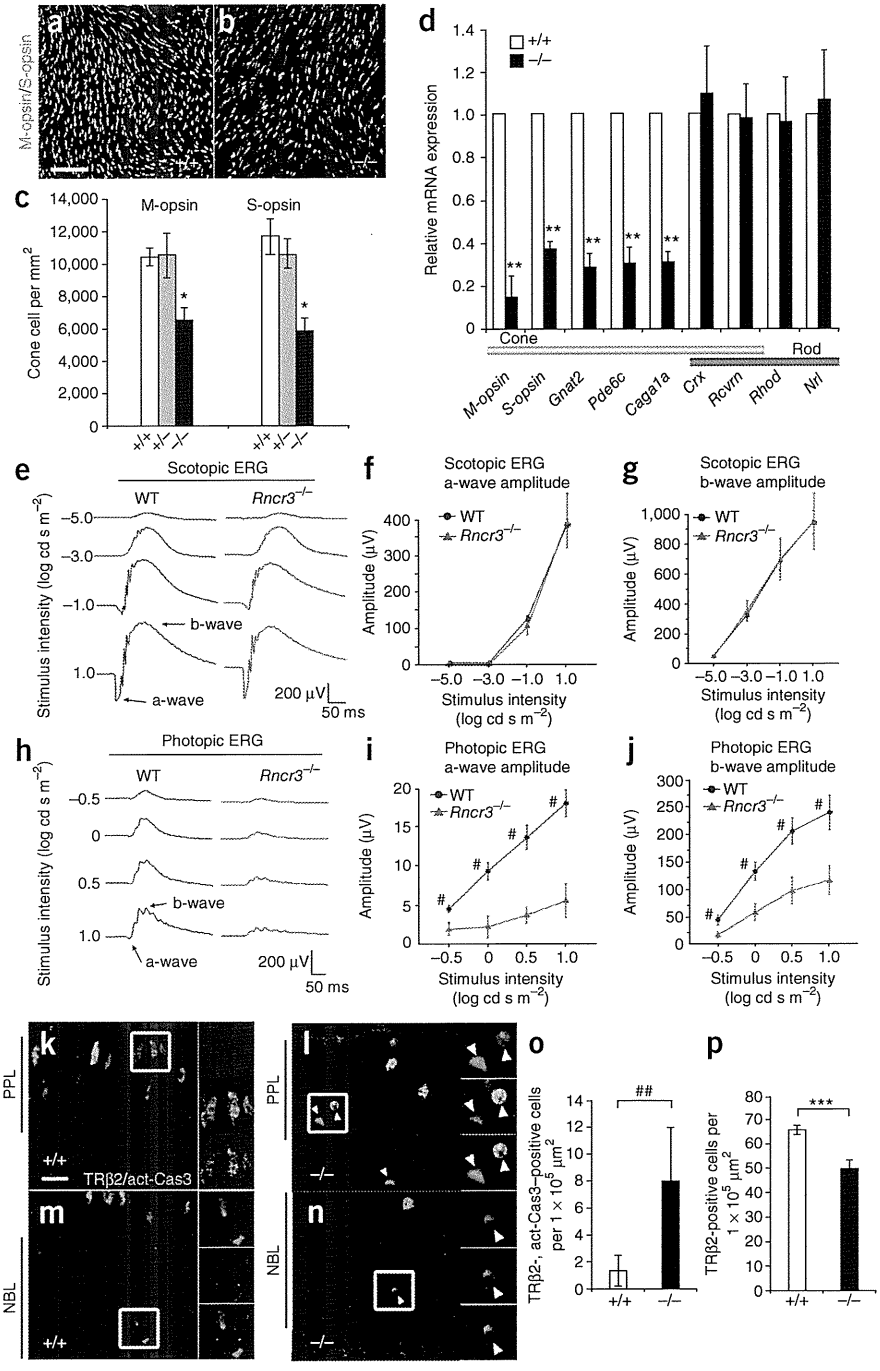

Figure 3 Reduction of cone photoreceptor cells in the *Rncr3*$^{-/-}$ retina. (**a**–**c**) Flat-mount immunostaining of central regions of wild-type (**a**) and *Rncr3*$^{-/-}$ (**b**) retinas using antibody to M-opsin (magenta) and antibody to S-opsin (green). Scale bar represents 50 μm. The number of cone cells expressing M-opsin and/or S-opsin in wild-type, *Rncr3*$^{+/-}$ and *Rncr3*$^{-/-}$ retinas are shown in **c** (*$P < 0.001$). Error bars represent s.d. from the means of triplicates. (**d**) Quantitative RT-PCR of retinal photoreceptor genes at P14 (**$P < 0.01$). Error bars represent s.d. from the means of three littermate pairs. *Actb* was used for normalization. (**e**–**j**) ERGs recorded from 2-month-old wild-type and *Rncr3*$^{-/-}$ mice. Scotopic ERGs elicited by four different stimulus intensities are shown in **e**. The amplitudes of the scotopic ERG a-wave (**f**) and the b-wave (**g**) are shown as a function of the stimulus intensity. Photopic ERGs elicited by four different stimulus intensities are shown in **h**. The amplitude of the photopic ERG a-wave (**i**) and the b-wave (**j**) are shown as a function of the stimulus intensity. Error bars represent s.e.m. (#$P < 0.05$). (**k**–**p**) Immunostaining of active caspase-3 (act-Cas3) and TRβ2 in the *Rncr3*$^{-/-}$ retina at P3. Arrowheads indicate active caspase-3 and TRβ2 double-positive cells. The white boxes indicate the area enlarged in the right panels. Scale bar represents 10 μm (**k**–**n**). The number of active caspase-3 and TRβ2 double-positive cells (**o**) and of TRβ2-positive cells (**p**) are shown. Error bars represent s.d. from the means of triplicates. ##$P < 0.02$, ***$P < 0.002$.

examined cell proliferation in the *Rncr3*$^{-/-}$ retina by immunostaining with phosphohistone H3 (PH3) and Ki67 and counting the number of PH3-positive cells at P3 (**Supplementary Fig. 7a–c**). The proportion of PH3-positive cells was not significantly different between wild-type and *Rncr3*$^{-/-}$ retinas ($P > 0.9$). These results suggest that miR-124a is necessary for proper survival and localization of cone cells rather than for early neurogenesis.

We found that 2-month-old *Rncr3*$^{-/-}$ mice had smaller brain weights than did wild types (**Fig. 4a,b**). The small brain phenotype was not apparent at P1, but became significant by P6 during maturation ($P < 0.005$, data not shown). Furthermore, *Rncr3*$^{-/-}$ mice exhibited a front and hind limb clasping response in the tail-suspension assay at 4–5 months (**Fig. 4c,d**). This abnormal phenotype is commonly observed in mouse models of neurodegenerative disorders[21], suggesting that the neural function of the *Rncr3*$^{-/-}$ mouse is substantially impaired. We then performed Timm staining on P10 wild-type and *Rncr3*$^{-/-}$ brain sections, the time at which mossy fibers develop[22], to examine dentate granule cell maturation (**Fig. 4e–h**). Notably, aberrant outgrowth of mossy fibers (dentate granule cell axons) into the CA3 region was observed in the *Rncr3*$^{-/-}$ mouse (**Fig. 4g,h**). The number of apoptotic cells in the dentate gyrus and cortex at P6 was significantly increased (dentate gyrus: wild type, 1.2 ± 1.6 cells per section; *Rncr3*$^{-/-}$, 10.2 ± 3.6; $P < 0.001$; cortex: wild type, 5.8 ± 2.5 cells per 5×10^5 μm^2; *Rncr3*$^{-/-}$, 59.4 ± 17.1; $P < 0.001$; **Fig. 4i–l**). Cell proliferation in the dentate gyrus of *Rncr3*$^{-/-}$ mice was not substantially affected (**Supplementary Fig. 7d,e**), suggesting that apoptosis of neurons contributes to the smaller brain size in *Rncr3*$^{-/-}$ mice. These results indicate that miR-124a is necessary for proper brain development and axogenesis of dentate granule neurons to the CA3.

Lhx2 is a direct target mRNA of miR-124a *in vivo*

To identify miR-124a target mRNAs, we searched for 3′ untranslated regions (UTRs) of genes that are highly expressed in retinal progenitors and substantially downregulated on progenitor differentiation[23], such as *Lhx2*, *Sox2*, *Rax*, *Six6*, *Six3*, *Pax2*, *Pax6*, *Vsx2* and *Otx2*, using TargetScan 5.1 (http://www.targetscan.org/). Searching the database revealed that *Lhx2* contains an evolutionarily

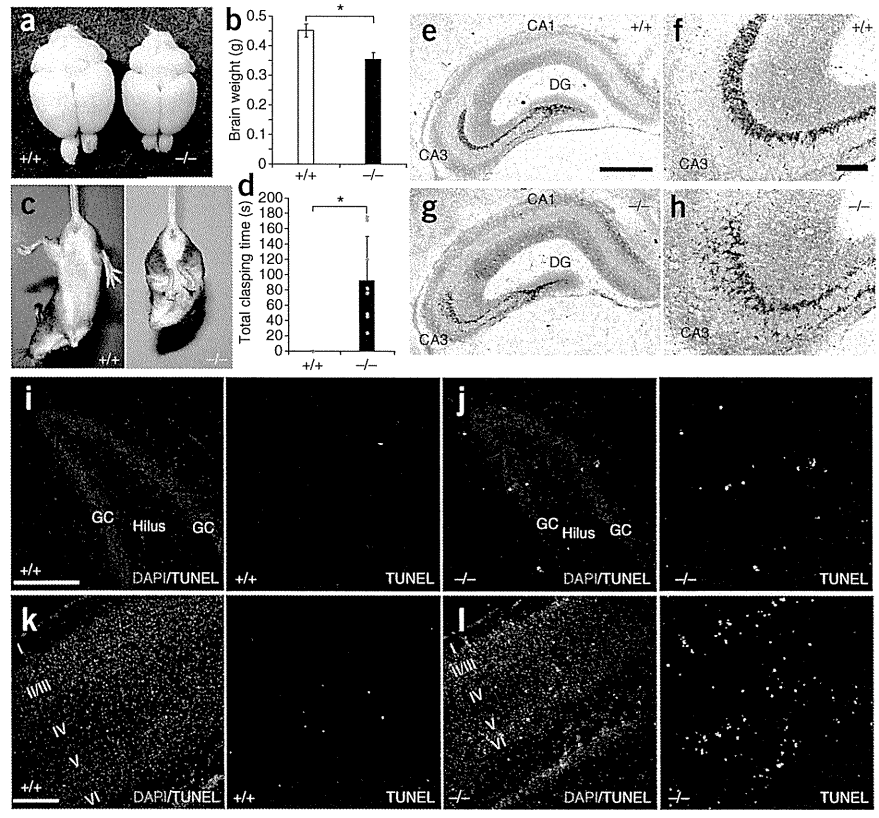

Figure 4 *Rncr3*$^{-/-}$ mice exhibit neuronal dysfunction and aberrant growth of dentate granule cell axon. (**a**,**b**) Appearance of the brain and brain weight in wild-type and *Rncr3*$^{-/-}$ mice. Representative brains from wild-type (left) and *Rncr3*$^{-/-}$ mice (right, litter mates, 2 months old) are shown in **a**. Brain weights of wild-type ($n = 5$) and *Rncr3*$^{-/-}$ mice ($n = 9$) are shown in **b** (*$P < 0.001$). Error bars represent s.d. (**c**,**d**) Abnormal limb-clasping of *Rncr3*$^{-/-}$ mouse. A clasping response was observed in the *Rncr3*$^{-/-}$ mouse (**c**, right), but not in the wild-type mouse (**c**, left). Total clasping time was measured for 3 min (**d**). Error bars represent s.d. from the mean of $n = 4$ (wild type) and $n = 8$ (*Rncr3*$^{-/-}$). (**e**–**h**) Aberrant sprouting of mossy fibers in the *Rncr3*$^{-/-}$ mouse. The mossy fiber terminals were visualized by Timm staining with Nissl counterstaining at P10. Scale bars represent 500 μm (**e**,**g**) and 100 μm (**f**,**h**). (**i**,**j**) TUNEL assay of the P6 wild-type and *Rncr3*$^{-/-}$ dentate gyrus. Scale bars represent 200 μm. (**k**,**l**) TUNEL assay of the P6 wild-type and *Rncr3*$^{-/-}$ visual cortex. Scale bars represent 200 μm. GC, granule cell layer.

highly conserved miR-124a target sequence (**Fig. 5a**). We examined whether *Lhx2* is a target mRNA of miR-124a by constructing luciferase reporter plasmids that contained native or mutated seed sequences of the *Lhx2* 3′ UTR (**Fig. 5a**) and co-transfecting these reporter plasmids with miR-124a expression plasmids (*pBAsi-mU6-miR-124a-1*, *pBAsi-mU6-miR-124a-2* or *pBAsi-mU6-miR-124a-3*) into HEK 293T cells that lacked endogenous miR-124a (**Supplementary Fig. 8a**,**b**). HEK 293T cells transfected with miR-124a expression plasmids produced significant amounts of miR-124a ($P < 0.001$; **Supplementary Fig. 8a**,**b**). The luciferase activity of the native *Lhx2* 3′-UTR plasmid was significantly reduced by all of the pre-miR-124a expression plasmids ($P < 0.01$; **Fig. 5b**). However, luciferase activity of the mutated *Lhx2* 3′-UTR plasmid was not attenuated by miR-124a (**Fig. 5b**), and the luciferase mRNA levels of both native and mutated *Lhx2* 3′-UTR plasmids were not significantly reduced ($P < 0.004$; **Supplementary Fig. 8c**,**d**). We observed a statistically significant increase of luciferase activity in *Rncr3*$^{-/-}$ hippocampal neurons transfected with native Lhx2 3′-UTR plasmid ($P < 0.009$), but found no significant effect in neurons transfected with the mutated *Lhx2* 3′-UTR plasmid ($P > 0.45$; **Supplementary Fig. 8e**). Next, to determine whether *Lhx2* is an *in vivo* target of miR-124a, we performed immunostaining of the E17.5 *Rncr3*$^{-/-}$ retina using antibodies to LHX2 and TRβ2 antibodies (**Fig. 5c–e**). The number of LHX2 and TRβ2 double-positive cells was significantly increased in the *Rncr3*$^{-/-}$ retina compared with the wild-type retina ($P < 0.01$; **Fig. 5e**). We then introduced *Lhx2* expression plasmids that contained native or mutated 3′ UTR (*Lhx2-Nat* and *Lhx2-Mut*) together with an *egfp* expression plasmid into the P0 mouse retina by *in vivo* electroporation to determine whether retinal cell apoptosis occurs by *Lhx2* overexpression. The number of TUNEL-positive cells was increased in retina transfected with the *Lhx2-Mut* plasmid, but transfection with the *Lhx2-Nat* plasmid did not lead to an increase in the number of TUNEL-positive cells (**Fig. 5f–h**), suggesting that the native 3′ UTR was targeted by native miR-124a. This result is consistent with the observation that the number of TUNEL-positive cells was significantly increased in the *Rncr3*$^{-/-}$ retina ($P < 0.05$; **Supplementary Fig. 6a–c**). These results suggest that *Lhx2* mRNA is a miR-124a target in the retina and that downregulation of *Lhx2* mRNA by miR-124a is necessary for retinal cell survival.

Lhx2 is known to be required for hippocampal formation[24]. We therefore conducted immunostaining on the dentate gyrus with antibodies to LHX2 and the dentate gyrus marker PROX1. The number of LHX2 and PROX1 double-positive cells was significantly increased in the *Rncr3*$^{-/-}$ dentate gyrus ($P < 0.001$; **Fig. 5i–k**). Furthermore, we compared the expression of *Rncr3* and *Lhx2* mRNA and LHX2 protein in the E12.5 forebrain and P3 retina (**Supplementary Fig. 8f–o**). At E12.5, *Lhx2* mRNA was highly expressed in both the hippocampus and thalamus, whereas *Rncr3* was highly expressed only in the thalamus. In both the developing brain and retina, LHX2 protein was not expressed in regions in which both *Lhx2* and *Rncr3* mRNA were expressed, suggesting that miR-124a targets *Lhx2* mRNA both in the retina and the brain and that miR-124a inhibits translation of *Lhx2* mRNA. Cell density was significantly higher in the dentate gyrus in *Rncr3*$^{-/-}$ mice than in wild-type mice, as determined by counting PROX1-positive cells ($P < 0.004$; **Fig. 5i**,**j**,**l**). To assess the role of *Lhx2* in aberrant mossy fiber sprouting, we electroporated *Lhx2-Nat* and *Lhx2-Mut* plasmids into primary cultured hippocampal cells. Substantial neurite extension was observed in cells expressing *Lhx2-Mut* (**Fig. 5m–o**). To evaluate axonal elongation in dentate granule cells, we immunostained hippocampal PROX1 neurons and then measured the axonal length of PROX1-positive cells (**Fig. 5p**,**q**). The percentage of neurons that contained longer axons, greater than 150 μm in length, was increased by expression of *Lhx2-Mut* (**Fig. 5p**). Furthermore, the average length of the neurons in the top 25th percentile of the population was also significantly increased in *Lhx2-Mut*–expression neurons ($P < 0.05$; **Fig. 5q**). We ectopically expressed *Lhx2* using lentivirus in P6 rat dentate gyrus in slice culture and found that *Lhx2*-transduced dentate granule cells extended longer

axons to the CA3 region by 5 d *in vitro* (DIV) than the wild-type cells (**Fig. 5r–u**). These results suggest that a proper LHX2 protein level, which is affected by miR-124a, is required for the appropriate development of axons in the dentate gyrus.

Rescue of *Rncr3*$^{-/-}$ mice by pre-miR-124a-2 or *Lhx2* knockdown

To determine whether miR-124a is responsible for the *Rncr3*$^{-/-}$ retinal phenotype, we carried out a rescue experiment by mating *Rncr3*$^{-/-}$ mice with transgenic mice that specifically expressed miR-124a in

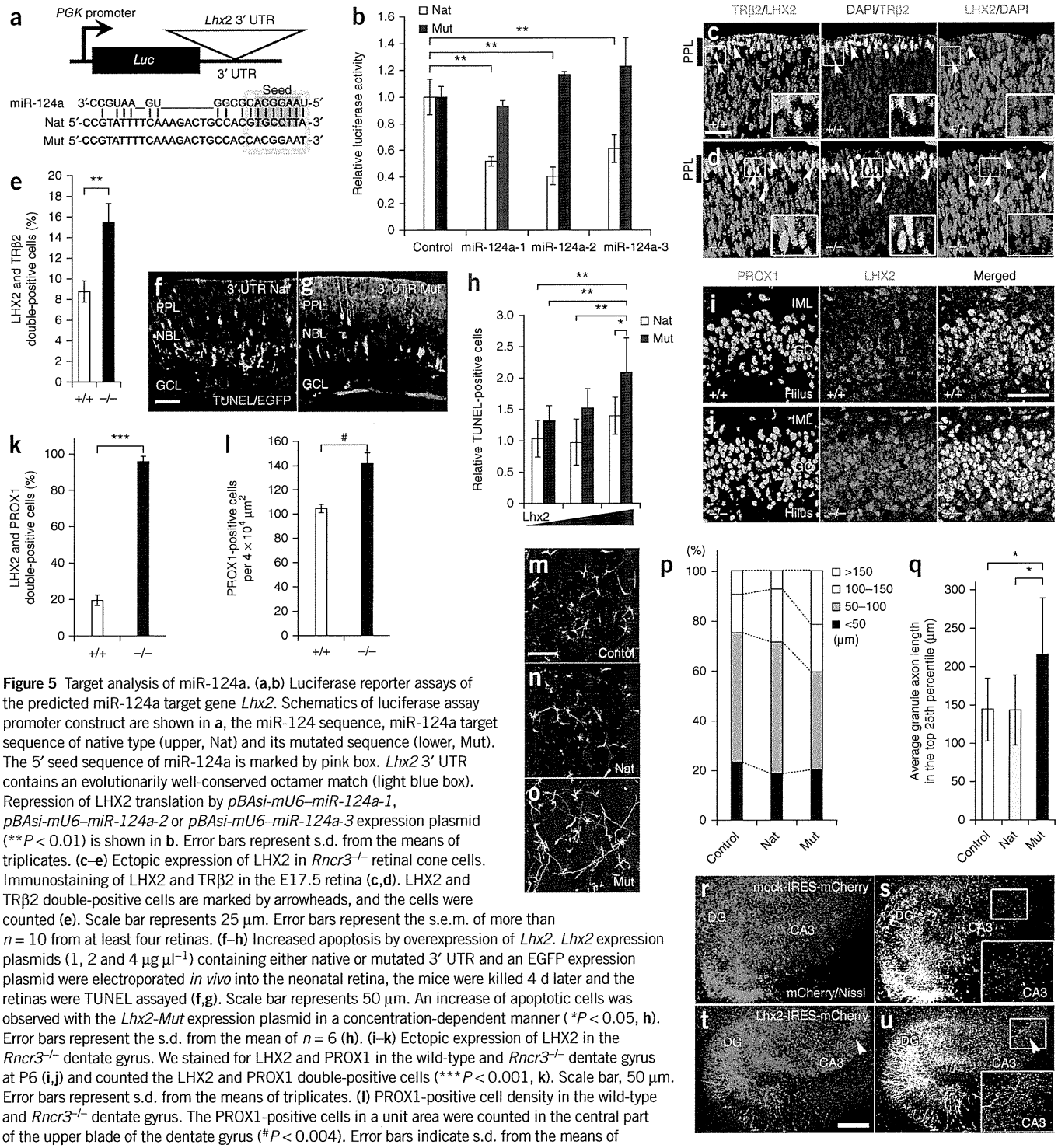

Figure 5 Target analysis of miR-124a. (**a**,**b**) Luciferase reporter assays of the predicted miR-124a target gene *Lhx2*. Schematics of luciferase assay promoter construct are shown in **a**, the miR-124 sequence, miR-124a target sequence of native type (upper, Nat) and its mutated sequence (lower, Mut). The 5′ seed sequence of miR-124a is marked by pink box. *Lhx2* 3′ UTR contains an evolutionarily well-conserved octamer match (light blue box). Repression of LHX2 translation by *pBAsi-mU6–miR-124a-1*, *pBAsi-mU6–miR-124a-2* or *pBAsi-mU6–miR-124a-3* expression plasmid (**$P < 0.01$) is shown in **b**. Error bars represent s.d. from the means of triplicates. (**c**–**e**) Ectopic expression of LHX2 in *Rncr3*$^{-/-}$ retinal cone cells. Immunostaining of LHX2 and TRβ2 in the E17.5 retina (**c**,**d**). LHX2 and TRβ2 double-positive cells are marked by arrowheads, and the cells were counted (**e**). Scale bar represents 25 μm. Error bars represent the s.e.m. of more than $n = 10$ from at least four retinas. (**f**–**h**) Increased apoptosis by overexpression of *Lhx2*. *Lhx2* expression plasmids (1, 2 and 4 μg μl^{-1}) containing either native or mutated 3′ UTR and an EGFP expression plasmid were electroporated *in vivo* into the neonatal retina, the mice were killed 4 d later and the retinas were TUNEL assayed (**f**,**g**). Scale bar represents 50 μm. An increase of apoptotic cells was observed with the *Lhx2-Mut* expression plasmid in a concentration-dependent manner (*$P < 0.05$, **h**). Error bars represent the s.d. from the mean of $n = 6$ (**h**). (**i**–**k**) Ectopic expression of LHX2 in the *Rncr3*$^{-/-}$ dentate gyrus. We stained for LHX2 and PROX1 in the wild-type and *Rncr3*$^{-/-}$ dentate gyrus at P6 (**i**,**j**) and counted the LHX2 and PROX1 double-positive cells (***$P < 0.001$, **k**). Scale bar, 50 μm. Error bars represent s.d. from the means of triplicates. (**l**) PROX1-positive cell density in the wild-type and *Rncr3*$^{-/-}$ dentate gyrus. The PROX1-positive cells in a unit area were counted in the central part of the upper blade of the dentate gyrus (#$P < 0.004$). Error bars indicate s.d. from the means of triplicates. (**m**–**q**) Axonal extension in *Lhx2-Mut*–expressing neurons. Primary hippocampal neurons from P0 mouse were transfected with mock (control), *Lhx2-Nat* (native), *Lhx2-Mut* (mutated) together with EGFP by electroporation. Confocal microimages of neurons 72 h after transfection are shown in **m**–**o**. Scale bar represents 200 μm. The percentages of axons with lengths ≤50, 50–100, 100–150 and >150 μm from $n = 85$ (control), 81 (nat), and 89 (mut) neurons are shown in **p**. The average axon lengths in the top 25% percentile are shown in **q**. Error bars represent s.d. (**r**–**u**) Lentivirus-infected hippocampal slice culture. Shown are confocal images of the P6, 5 DIV sliced rat hippocampus infected with mock (control, **r**,**s**) or *Lhx2* (**t**,**u**) expression virus. The small white boxes in **s** and **u** are the CA3 regions, magnified in the bottom right corner. Arrowheads indicate elongated mossy fibers in the CA3. Scale bar represents 200 μm. IML, inner molecular layer.

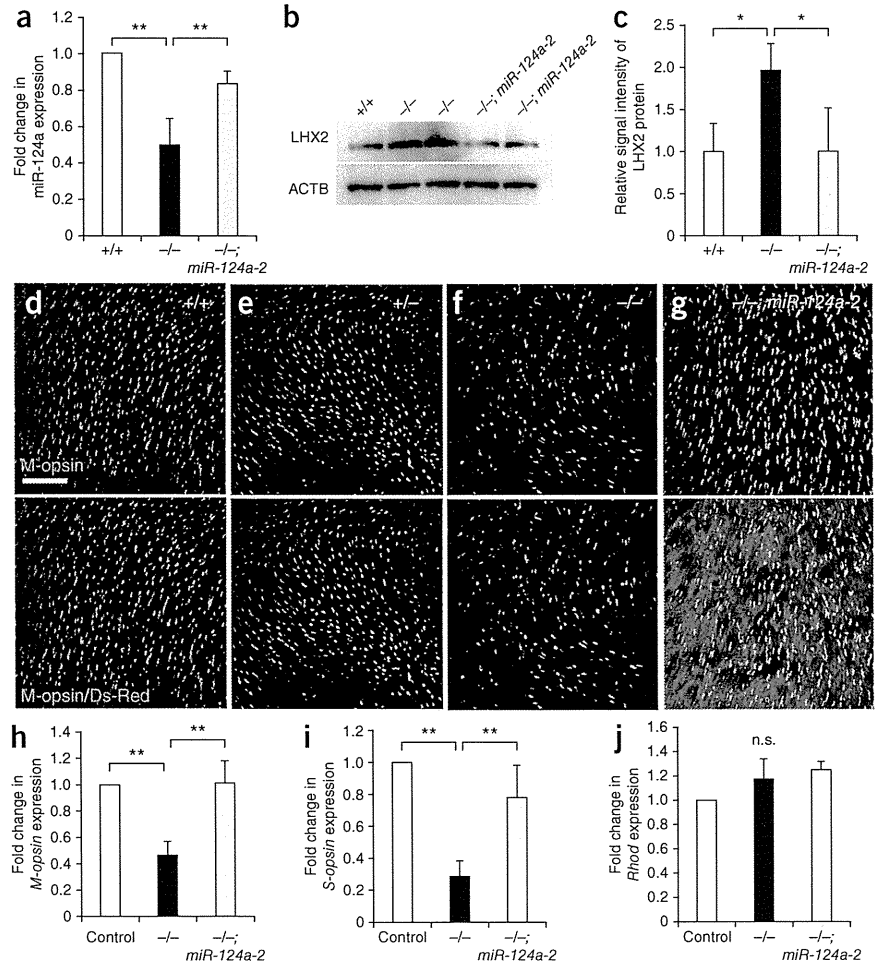

Figure 6 *In vivo* rescue experiments of *Rncr3*$^{-/-}$ mice by miR-124a expression in the retina. (**a**) Expression of miR-124a in the wild-type, *Rncr3*$^{-/-}$ and *Rncr3*$^{-/-}$; *Crx–miR-124a-2* retinas (**$P < 0.01$). Error bars represent the s.d. from the mean of triplicate (wild type and *Rncr3*$^{-/-}$) and $n = 4$ (*Rncr3*$^{-/-}$; *Crx–miR-124a-2*). (**b**,**c**) Comparison of LHX2 protein levels in the wild-type, *Rncr3*$^{-/-}$ and *Rncr3*$^{-/-}$; *Crx–miR-124a-2* retina. Western blots of LHX2 in the retina are shown in **b**. ACTB (β-actin) was used as a loading control. The signal intensity of LHX2 protein is shown in **c** (*$P < 0.05$). Error bars represent the s.d. from the means of triplicates (wild type) and $n = 4$ (*Rncr3*$^{-/-}$ and *Rncr3*$^{-/-}$; *Crx–miR-124a-2*). (**d–g**) Rescue of decreased cone cells by miR-124a expression. Flat-mount immunostaining using antibody to M-opsin (green). The *pre-miR-124a-2* transgene also expressed Ds-Red (magenta) as a marker. Scale bar represents 50 μm. (**h–j**) Real-time qRT-PCR analysis of control (+/+; *Crx–miR-124a-2* and *Rncr3*$^{+/-}$; *Crx–miR-124a-2*), *Rncr3*$^{-/-}$ and *Rncr3*$^{-/-}$; *Crx–miR-124a-2* transgenic retinas. Intron-spanning primers amplifying mouse *M-opsin* (also known as *Opn1mw*, **h**), *S-opsin* (also known as *Opn1sw*, **i**), *Rho* (**j**), and *Actb* were used for normalization. Error bars represent the s.d. from the means of three independent littermate pairs. **$P < 0.01$; n.s., not significant, $P > 0.05$.

photoreceptor cells using a *Ds-Red-intron-miR-124a-2* expression cassette driven by 2.3 kb of the *Crx* promoter[5,25] (*Crx–miR-124a-2*; **Supplementary Fig. 9a**). In the P1 retina, we observed that both miR-124a expression and the LHX2 protein level reverted back to those of control mice (**Fig. 6a–c**). We then performed flat-mount immunostaining (**Fig. 6d–g**) and conducted qPCR analysis on retinal photoreceptor marker genes using the adult retina (**Fig. 6h–j**). Both the decreased cone cell numbers and gene expression in the *Rncr3*$^{-/-}$ retina were restored to normal levels when transgenic pre-miR-124a-2 was expressed (**Fig. 6d–i**). The number of mislocalized cone cells also recovered (**Supplementary Fig. 9b–i**). These results suggest that the cone cell reduction and mislocalization in the *Rncr3*$^{-/-}$ retina are the results of miR-124a-1 disruption and that the primary function of *Rncr3* is to encode miR-124a.

To determine whether the loss of miR-124a is also responsible for the brain phenotypes, we generated a transgenic mouse that expresses *Ds-Red-intron-miR-124a-2* in postmitotic neurons, driven by 4.3 kb of the *synapsin 1* promoter (*Syn1–miR-124a-2*)[26] (**Supplementary Fig. 10a–c**). We performed an *in situ* hybridization of miR-124a and immunostained for LHX2 in the P10 brain. In the dentate gyrus of the *Rncr3*$^{-/-}$; *Syn1–miR-124a-2* mice, both the reduced level of mature miR-124a and the elevated level of LHX2 protein that we observed in *Rncr3*$^{-/-}$ mice were restored to similar levels as seen in control mice (**Fig. 7a–f**). In addition, the number of apoptotic cells was significantly reduced in the brains of *Rncr3*$^{-/-}$; *Syn1–miR-124a-2* mice compared with *Rncr3*$^{-/-}$ mice ($P < 0.01$; **Supplementary Fig. 10d**). In *Rncr3*$^{-/-}$; *Syn1–miR-124a-2* mice, Timm-stained mossy fiber axonal terminals incompletely, but substantially, recovered from aberrant sprouting into the CA3 region (**Fig. 7g–l**). The other phenotypes, including brain weight, clasping and apoptosis in the cortex, were not substantially rescued in *Rncr3*$^{-/-}$; *Syn1–miR-124a-2* mice (data not shown). This partial rescue may be a result of insufficient expression and/or inappropriate expression timing of the miR-124a transgene.

To determine whether downregulation of *Lhx2* can rescue the *Rncr3*$^{-/-}$ phenotype, we constructed a short hairpin RNA (shRNA) to knockdown *Lhx2* (*shLhx2*; **Supplementary Fig. 11a,b**). We transfected *shLhx2* into organ-cultured P0 retina using a recombinant adeno-associated virus serotype 5 (AAV5; **Supplementary Fig. 11c**). After 5 DIV, we performed immunostaining using an antibody to S-opsin. In the 5 DIV *Rncr3*$^{-/-}$ retina, the number of cone cells was reduced in retina transfected with control shRNA (shControl), whereas the number of cone cells was significantly increased in retina transfected with *shLhx2* compared with the control ($P < 0.01$; **Fig. 8a–e**). The number of cone cells in *shLhx2*-infected wild-type retina was unaltered (**Fig. 8a,c**), suggesting that the *Lhx2* knockdown rescue phenotype is not a result of an off-target effect. In addition, we forced the expression of shLhx2 in primary cultured hippocampal neurons to determine whether downregulation of *Lhx2* can rescue *Rncr3*$^{-/-}$ dentate gyrus neuron axonal elongation (**Fig. 8f–j**). The average dentate granular axon length in the neurons in the top 25th percentile of the population (determined by axon length) was significantly increased in shControl-transfected *Rncr3*$^{-/-}$ dentate gyrus neurons ($P < 0.01$; **Fig. 8g**). The elongated *Rncr3*$^{-/-}$ dentate gyrus axon phenotype was restored to the wild-type level by transfection of *shLhx2* (**Fig. 8i,j**). These results suggest that *Lhx2* is a primary target gene of miR-124a and is responsible for the *Rncr3*$^{-/-}$ phenotypes, including both the reduction of retinal cone cell numbers and mossy fiber elongation of the dentate gyrus.

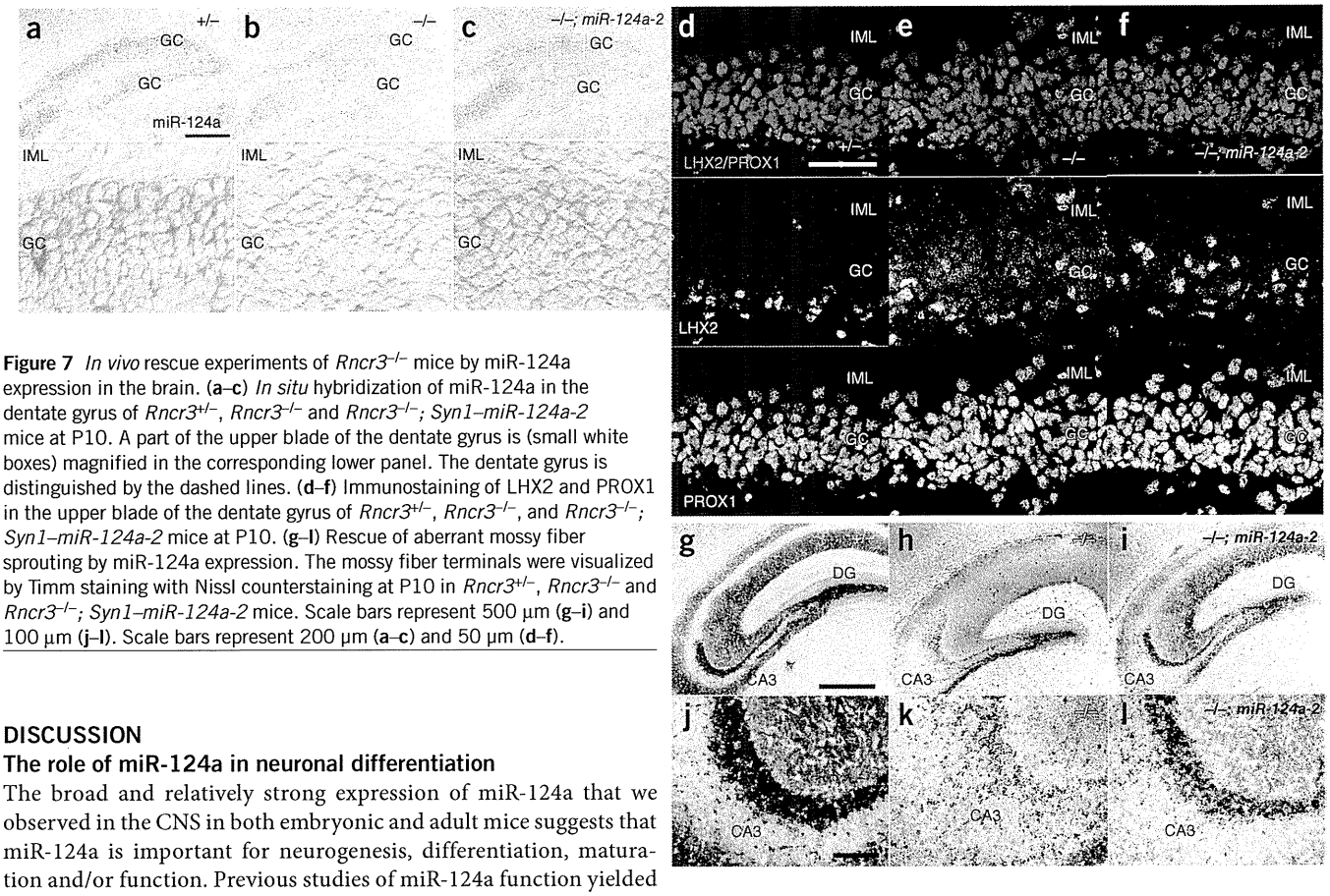

Figure 7 *In vivo* rescue experiments of *Rncr3*$^{-/-}$ mice by miR-124a expression in the brain. (**a–c**) *In situ* hybridization of miR-124a in the dentate gyrus of *Rncr3*$^{+/-}$, *Rncr3*$^{-/-}$ and *Rncr3*$^{-/-}$*; Syn1–miR-124a-2* mice at P10. A part of the upper blade of the dentate gyrus is (small white boxes) magnified in the corresponding lower panel. The dentate gyrus is distinguished by the dashed lines. (**d–f**) Immunostaining of LHX2 and PROX1 in the upper blade of the dentate gyrus of *Rncr3*$^{+/-}$, *Rncr3*$^{-/-}$, and *Rncr3*$^{-/-}$*; Syn1–miR-124a-2* mice at P10. (**g–l**) Rescue of aberrant mossy fiber sprouting by miR-124a expression. The mossy fiber terminals were visualized by Timm staining with Nissl counterstaining at P10 in *Rncr3*$^{+/-}$, *Rncr3*$^{-/-}$ and *Rncr3*$^{-/-}$*; Syn1–miR-124a-2* mice. Scale bars represent 500 μm (**g–i**) and 100 μm (**j–l**). Scale bars represent 200 μm (**a–c**) and 50 μm (**d–f**).

DISCUSSION

The role of miR-124a in neuronal differentiation

The broad and relatively strong expression of miR-124a that we observed in the CNS in both embryonic and adult mice suggests that miR-124a is important for neurogenesis, differentiation, maturation and/or function. Previous studies of miR-124a function yielded inconsistent results. A previous study found that miR-124a did not act as a determinant of neuronal generation through both knockdown and overexpression experiments of miR-124a in the developing chick neural tube[7]. In contrast, another study found that miR-124a is required for neuronal determination in the developing chick neural tube[4]. Studies using *Dicer* conditional knockout mice have shown that miRNA is not necessary for neuronal determination[8,9]. In *Xenopus*, a knockdown experiment by micro-injection of locked nucleic acid (LNA)–modified anti–miR-124a oligonucleotides into the eight-cell stage revealed no obvious effect[27]. We observed normal neurogenesis in the developing photoreceptor layer and the dentate gyrus in *Rncr3*$^{-/-}$ mice in which miR-124a expression is mostly eliminated. These results are consistent with previous reports that miR-124a is expressed in the Ki67-negative postmitotic cells and regulated by the REST complex[6,28], suggesting that miR-124a functions in neuronal maturation and maintenance, rather than neuronal determination (**Supplementary Fig. 12**). It will be important to examine the role of miR-124a in neuronal determination and maturation in the future,

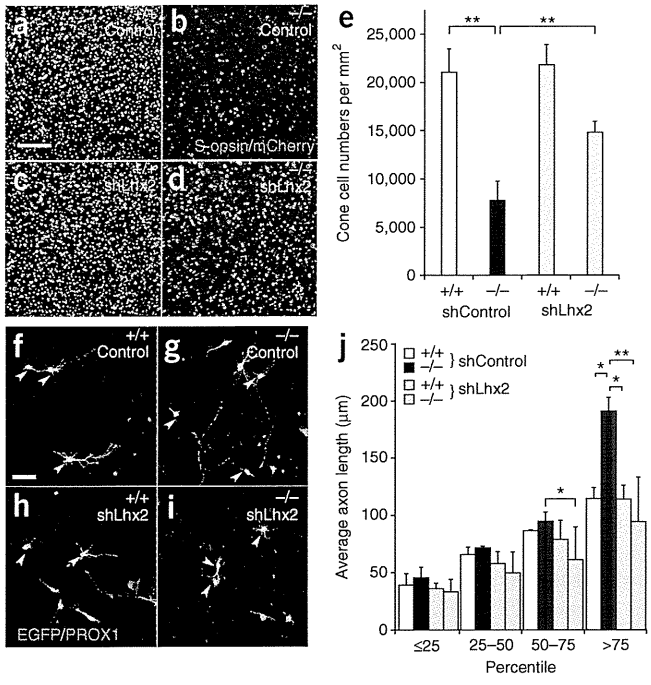

Figure 8 Rescue of *Rncr3*$^{-/-}$ mice by pre-miR-124a-2 expression. (**a–e**) Flat-mount immunostaining of S-opsin in the 5 DIV cultured retina. P0 wild-type (**a**,**c**) and *Rncr3*$^{-/-}$ retinas (**b**,**d**) were dissected and transfected with *U6* promoter–driven *shControl* (**a**,**b**) or *shLhx2* (**c**,**d**) with bicistronic expression of *CMV-mCherry* using AAV5 (**a–d**). Scale bar represents 50 μm. We counted the numbers of S-opsin–positive cone cell (**$P < 0.01$, **e**). Error bars represent s.d. from the means of $n = 4$. (**f–j**) Axon length of dentate granule cells after 70 h culture. P0 hippocampus of wild-type and *Rncr3*$^{-/-}$ mice were isolated and dissociated, then transfected with a *pBAsi-shControl* or *pBAsi-shLhx2-3* plasmid together with a *pCAG-egfp* plasmid. After immunostaining for PROX1 and EGFP, confocal fluorescence images were obtained. Scale bar represents 50 μm (**f–i**). The average axon length were calculated in 0–25th, 25–50th, 50–75th and 75–100th percentile groups (*$P < 0.05$ and **$P < 0.01$, **j**). Error bars represent s.d. from the means of $n = 3$. A total of 243 neurons were measured.

and analysis of pre-miR-124a-1 and pre-miR-124a-2 double knockout or miR-124a-1, miR-124a-2 and miR-124a-3 triple knockout mice will be necessary to draw a definitive conclusion.

Although the number of cone cells was significantly reduced in *Rncr3*$^{-/-}$ mice ($P < 0.001$), rod photoreceptor cells did not seem to be significantly affected ($P > 0.65$; **Fig. 3c,d** and **Supplementary Fig. 4a**). When we expressed a pre-miR-124a-2 transgene in the developing photoreceptors of *Rncr3*$^{-/-}$ mice, the number of cone cells was increased (**Fig. 6d–i**), suggesting that rod cells and other retinal neurons compensate for miR-124a loss with pre-miR-124a-2. Previous studies of the *Dicer* conditional knockout mouse in the retina suggested that photoreceptor differentiation at late developmental stages requires miRNAs[9] and that, of the retinal cell types, photoreceptors are the most sensitive to an imbalance of miRNAs[29]. Our results suggest that miR-124a is one of the main miRNAs functioning in photoreceptor cell maturation.

In vivo miR-124a target mRNAs

Several groups identified target mRNAs of miR-124a in the CNS using translation assay and *in vivo* knockdown analysis. It was recently suggested that CREB1 and *Actl6a* (*BAF53a*) are miR-124a target mRNAs in *Aplysia* and mouse, respectively[30,31]. *Sox9* was also reported to be a miR-124a target in SVZ adult neurogenesis[6]. *Ptbp1* and *Ctdsp1* were reported to be targets of miR-124a and are involved in neuronal gene regulation in cultured cells[4,5]. The pairing mechanism between miRNA and target mRNA is well established as a Watson-Crick pairing known as the miRNA seed match (especially nucleotides 2–7)[32–34]. Furthermore, it was recently found that guanidine:uridine wobble base-pairing between miRNA seed region and mRNA interferes with targeting activity[35]. Taking advantage of recently updated database information, we re-examined reported miR-124a targets using TargetScan 5.1 and found *Lhx2*, a miR-124a target mRNA candidate in both humans and mice, as well as *Ptbp1*, and *Ctdsp1*. Although *Lhx2* or *Neurod1* were predicted to be miR-124a target mRNAs by a miR-124a overexpression experiment in *Xenopus*[27,36], precursor miRNA overexpression may mistakenly produce a phenotype as a result of an effect on the miRNA synthesis mechanism or off-target effects. In fact, we did not detect a significant change in NEUROD1 protein and *Otx2* transcript expression ($P > 0.79$; **Fig. 2i–l** and **Supplementary Fig. 5g,k,n**), both of which were affected by pre-miR-124a overexpression in the *Xenopus* study[27,36]. Here, we found that *Lhx2* is a target of miR-124a in retinal cones and in the dentate gyrus in *Rncr3*$^{-/-}$ mice (**Fig. 5** and **Supplementary Fig. 8a–d**). Furthermore, LHX2 protein localization did not overlap with *Lhx2* mRNA distribution in regions in which *Rncr3* was expressed (**Supplementary Fig. 8f–o**). These observations suggest that LHX2 protein expression is affected by miR-124a by translational inhibition. We also performed both a luciferase assay and qPCR of luciferase mRNA (**Supplementary Fig. 8c,d**). Notably, although the luciferase activity of the construct containing a miR-124a target sequence in its 3′ UTR was decreased by miR-124a expression, the level of luciferase mRNA was unchanged. Our *Lhx2* overexpression assay revealed that cell death was increased in the developing retina, suggesting that inhibition of *Lhx2* translation by miR-124a is one of the essential mechanisms for down-regulating *Lhx2* in the normal development of retinal cells (**Supplementary Fig. 12**).

Lhx2 functions as a selector gene for forebrain and eye development[37]. *Lhx2*-expressing normal dorsal telencephalon cells show a marked tendency to form aggregation clusters[24], implying that LHX2 contributes to the regionalization of the cortical hem (LHX2 negative) and the non–cortical hem hippocampal region (LHX2 positive)[24]. In the *Rncr3*$^{-/-}$ brain, elevation of LHX2 protein levels may lead to a higher density of dentate neurons by promoting cell aggregation (**Fig. 5i,j,l**). Furthermore, we observed aberrant sprouting of dentate gyrus axons, mossy fibers, into the CA3 region in the *Rncr3*$^{-/-}$ brain (**Fig. 4e–h**), and found that the LHX2 level affects axonal outgrowth in primary cultured hippocampal dentate neurons (**Figs. 5m–u** and **8f–j**). It was recently shown that commissural neurons, which express LHX2 protein, extend their axons, but fail to cross the midline in *Lhx2* and *Lhx9* double knockout mice, suggesting that *Lhx2*-defective commissural neurons do not respond well to guidance cues[38]. In contrast, in the CA3 region of the *Rncr3*$^{-/-}$ hippocampus, we hypothesize that dentate gyrus granule cells may have an axon elongation capability and may over-respond to guidance cues, resulting in the mis-sprouting of granule cells to the CA3 region. Although elevated LHX2 may induce the aberrant axonal elongation phenotype, it should be noted that increased cell density and aberrant sprouting of dentate neurons in the hippocampus have been observed in seizure-induced rats[39]. Thus, understanding the precise mechanism that underlies these phenotypes awaits future study. Taken together, our findings suggest that LHX2 protein level regulation by miR-124a is critical for dentate gyrus maturation and survival (**Supplementary Fig. 12**).

Implication of miR-124a in human diseases

In humans, pre-miR-124a-1 is located on chromosome 8p23.1. Notably, chromosomal duplication, deletion or mutation of the 8p23.1 region have been reported to be involved in cerebral development and neuropsychiatric disorders, including autism, bipolar disorder, schizophrenia, learning difficulties, epilepsy and microcephaly[2,40,41]. In individuals with temporal lobe epilepsy and model animals, aberrantly sprouting mossy fibers are often observed[42]. However, the molecular mechanisms remain unknown. We found that a substantial reduction or loss of mature miR-124a (by 60–80%) or loss of miR-124a-1 resulted in a small brain, neuronal dysfunction and aberrant axonal sprouting in the hippocampus (**Fig. 4**), suggesting that dis-regulation of the miR-124a expression level is involved in developmental neuropsychiatric disorders and temporal lobe epilepsy in humans with chromosome 8p abnormalities.

A recent study of FMRP, a protein that is involved in a fragile X syndrome and a RISC component interacting with Argonaute, suggested that miR-124a interacts with the FMRP protein, which is present at synapses[43,44]. It was recently reported that miR-124a is bound and regulated by dFMR1, a FMRP protein in *Drosophila*[45]. Another study found that miR-124a is present in sensory-motor synapses and is involved in synaptic plasticity through CREB in *Aplysia*[30]. Thus, it was suggested that miR-124a is important for synaptic function. In contrast, it should be noted that another study using rat hippocampal neurons found that mature miR-124a is not enriched in synaptosomes[46]. Further analysis will be needed to fully understand the role of miR-124a in synaptic functions.

There are three pre-miR-124a loci (pre-miR-124a-1, pre-miR-124a-2 and pre-miR-124a-3) in the mouse and human genomes. Our findings strongly suggest that *Rncr3* is the primary source of miR-124a. Production and analysis of miR-124a double and/or triple knockout mice, if the mutations are not lethal, will further clarify *in vivo* miR-124a function and target mRNAs in other parts of the CNS.

METHODS

Methods and any associated references are available in the online version of the paper at http://www.nature.com/natureneuroscience/.

Note: Supplementary information is available on the Nature Neuroscience website.

ACKNOWLEDGMENTS

We thank T. Maniatis for *RIPmiR-124a-2*, M. Kilimann for *Synapsin 1* promoter, Y. Omori, K. Terada, M. Ueno, N. Nagata, K. Aritake, Y. Oishi, T. Hamasaki, and H. Abe for critical comments and technical advice, and A. Tani, M. Kadowaki, Y. Kawakami, A. Ishimaru, H. Tsujii, T. Saioka, K. Sone, H. Abe, and S. Kennedy for technical assistance. This work was supported by Japan Science and Technology Agency (JST), Core Research for Evolutional Science and Technology (CREST), Grant-in-Aid for Scientific Research (B), Grant-in-Aid for Young Scientists (B), a Grant for Molecular Brain Science from the Ministry of Education, Culture, Sports, Science and Technology, the Takeda Science Foundation, the Uehara Memorial Foundation, the Mochida Memorial Foundation, and the Naito Foundation.

AUTHOR CONTRIBUTIONS

R.S. and T.F. designed the project. R.S., C.K., S.W., S.I. and T.F carried out the molecular and *in situ* hybridization experiments. R.S. and A.O. performed *in vivo* electroporation, virus infection and knockdown experiments in retinal and hippocampal neurons, and immunohistochemistry. S.U., T.K., M.K. and R.S. carried out the ERG experiments. R.S., Y.M. and T.F. produced the knockout and transgenic mice. R.S., R. Muramatsu and T.Y. carried out hippocampal tissue experiments. R.S., R. Matsui and D.W. produced lentivirus. R.S., Y.C. and Y.U. produced adeno-associated virus. R.S. and T.F. wrote the manuscript. T.F. supervised the project.

COMPETING FINANCIAL INTERESTS

The authors declare no competing financial interests.

Published online at http://www.nature.com/natureneuroscience/.
Reprints and permissions information is available online at http://www.nature.com/reprints/index.html.

1. Lagos-Quintana, M. *et al.* Identification of tissue-specific microRNAs from mouse. *Curr. Biol.* **12**, 735–739 (2002).
2. Tabarés-Seisdedos, R. & Rubenstein, J.L. Chromosome 8p as a potential hub for developmental neuropsychiatric disorders: implications for schizophrenia, autism and cancer. *Mol. Psychiatry* **14**, 563–589 (2009).
3. Lim, L.P. *et al.* Microarray analysis shows that some microRNAs downregulate large numbers of target mRNAs. *Nature* **433**, 769–773 (2005).
4. Visvanathan, J., Lee, S., Lee, B., Lee, J.W. & Lee, S.K. The microRNA miR-124 antagonizes the anti-neural REST/SCP1 pathway during embryonic CNS development. *Genes Dev.* **21**, 744–749 (2007).
5. Makeyev, E.V., Zhang, J., Carrasco, M.A. & Maniatis, T. The microRNA miR-124 promotes neuronal differentiation by triggering brain-specific alternative pre-mRNA splicing. *Mol. Cell* **27**, 435–448 (2007).
6. Cheng, L.C., Pastrana, E., Tavazoie, M. & Doetsch, F. miR-124 regulates adult neurogenesis in the subventricular zone stem cell niche. *Nat. Neurosci.* **12**, 399–408 (2009).
7. Cao, X., Pfaff, S.L. & Gage, F.H. A functional study of miR-124 in the developing neural tube. *Genes Dev.* **21**, 531–536 (2007).
8. De Pietri Tonelli, D. *et al.* miRNAs are essential for survival and differentiation of newborn neurons but not for expansion of neural progenitors during early neurogenesis in the mouse embryonic neocortex. *Development* **135**, 3911–3921 (2008).
9. Georgi, S.A. & Reh, T.A. Dicer is required for the transition from early to late progenitor state in the developing mouse retina. *J. Neurosci.* **30**, 4048–4061 (2010).
10. Koike, C. *et al.* TRPM1 is a component of the retinal ON bipolar cell transduction channel in the mGluR6 cascade. *Proc. Natl. Acad. Sci. USA* **107**, 332–337 (2010).
11. Blackshaw, S. *et al.* Genomic analysis of mouse retinal development. *PLoS Biol.* **2**, e247 (2004).
12. He, S. *et al.* MicroRNA-encoding long non-coding RNAs. *BMC Genomics* **9**, 236 (2008).
13. Hackler, L., Wan, J., Swaroop, A., Qian, J. & Zack, D.J. MicroRNA profile of the developing mouse retina. *Invest. Ophthalmol. Vis. Sci.* **51**, 1823–1831 (2010).
14. Ohsawa, R. & Kageyama, R. Regulation of retinal cell fate specification by multiple transcription factors. *Brain Res.* **1192**, 90–98 (2008).
15. Cepko, C.L., Austin, C.P., Yang, X., Alexiades, M. & Ezzeddine, D. Cell fate determination in the vertebrate retina. *Proc. Natl. Acad. Sci. USA* **93**, 589–595 (1996).
16. Ng, L. *et al.* A thyroid hormone receptor that is required for the development of green cone photoreceptors. *Nat. Genet.* **27**, 94–98 (2001).
17. Furukawa, T., Morrow, E.M. & Cepko, C.L. Crx, a novel otx-like homeobox gene, shows photoreceptor-specific expression and regulates photoreceptor differentiation. *Cell* **91**, 531–541 (1997).
18. Chen, S. *et al.* Crx, a novel Otx-like paired-homeodomain protein, binds to and transactivates photoreceptor cell-specific genes. *Neuron* **19**, 1017–1030 (1997).
19. Nishida, A. *et al.* Otx2 homeobox gene controls retinal photoreceptor cell fate and pineal gland development. *Nat. Neurosci.* **6**, 1255–1263 (2003).
20. Silber, J. *et al.* miR-124 and miR-137 inhibit proliferation of glioblastoma multiforme cells and induce differentiation of brain tumor stem cells. *BMC Med.* **6**, 14 (2008).
21. Côté, F., Collard, J.F. & Julien, J.P. Progressive neuronopathy in transgenic mice expressing the human neurofilament heavy gene: a mouse model of amyotrophic lateral sclerosis. *Cell* **73**, 35–46 (1993).
22. Okazaki, M.M., Evenson, D.A. & Nadler, J.V. Hippocampal mossy fiber sprouting and synapse formation after status epilepticus in rats: visualization after retrograde transport of biocytin. *J. Comp. Neurol.* **352**, 515–534 (1995).
23. Chow, R.L. & Lang, R.A. Early eye development in vertebrates. *Annu. Rev. Cell Dev. Biol.* **17**, 255–296 (2001).
24. Mangale, V.S. *et al.* Lhx2 selector activity specifies cortical identity and suppresses hippocampal organizer fate. *Science* **319**, 304–309 (2008).
25. Furukawa, A., Koike, C., Lippincott, P., Cepko, C.L. & Furukawa, T. The mouse Crx 5′-upstream transgene sequence directs cell-specific and developmentally regulated expression in retinal photoreceptor cells. *J. Neurosci.* **22**, 1640–1647 (2002).
26. Hoesche, C., Sauerwald, A., Veh, R.W., Krippl, B. & Kilimann, M.W. The 5′-flanking region of the rat synapsin I gene directs neuron-specific and developmentally regulated reporter gene expression in transgenic mice. *J. Biol. Chem.* **268**, 26494–26502 (1993).
27. Qiu, R. *et al.* The role of miR-124a in early development of the *Xenopus* eye. *Mech. Dev.* **126**, 804–816 (2009).
28. Conaco, C., Otto, S., Han, J.J. & Mandel, G. Reciprocal actions of REST and a microRNA promote neuronal identity. *Proc. Natl. Acad. Sci. USA* **103**, 2422–2427 (2006).
29. Damiani, D. *et al.* Dicer inactivation leads to progressive functional and structural degeneration of the mouse retina. *J. Neurosci.* **28**, 4878–4887 (2008).
30. Rajasethupathy, P. *et al.* Characterization of small RNAs in aplysia reveals a role for miR-124 in constraining synaptic plasticity through CREB. *Neuron* **63**, 803–817 (2009).
31. Yoo, A.S., Staahl, B.T., Chen, L. & Crabtree, G.R. MicroRNA-mediated switching of chromatin-remodeling complexes in neural development. *Nature* **460**, 642–646 (2009).
32. Friedman, R.C., Farh, K.K., Burge, C.B. & Bartel, D.P. Most mammalian mRNAs are conserved targets of microRNAs. *Genome Res.* **19**, 92–105 (2009).
33. Lewis, B.P., Burge, C.B. & Bartel, D.P. Conserved seed pairing, often flanked by adenosines, indicates that thousands of human genes are microRNA targets. *Cell* **120**, 15–20 (2005).
34. Lewis, B.P., Shih, I.H., Jones-Rhoades, M.W., Bartel, D.P. & Burge, C.B. Prediction of mammalian microRNA targets. *Cell* **115**, 787–798 (2003).
35. Doench, J.G. & Sharp, P.A. Specificity of microRNA target selection in translational repression. *Genes Dev.* **18**, 504–511 (2004).
36. Liu, K. *et al.* MiR-124 regulates early neurogenesis in the optic vesicle and forebrain, targeting NeuroD1. *Nucleic Acids Res.* **39**, 2869–2879 (2011).
37. Porter, F.D. *et al.* Lhx2, a LIM homeobox gene, is required for eye, forebrain and definitive erythrocyte development. *Development* **124**, 2935–2944 (1997).
38. Wilson, S.I., Shafer, B., Lee, K.J. & Dodd, J. A molecular program for contralateral trajectory: Rig-1 control by LIM homeodomain transcription factors. *Neuron* **59**, 413–424 (2008).
39. Holmes, G.L., Sarkisian, M., Ben-Ari, Y. & Chevassus-Au-Louis, N. Mossy fiber sprouting after recurrent seizures during early development in rats. *J. Comp. Neurol.* **404**, 537–553 (1999).
40. Baulac, S. *et al.* A novel locus for generalized epilepsy with febrile seizures plus in French families. *Arch. Neurol.* **65**, 943–951 (2008).
41. Glancy, M. *et al.* Transmitted duplication of 8p23.1–8p23.2 associated with speech delay, autism and learning difficulties. *Eur. J. Hum. Genet.* **17**, 37–43 (2009).
42. Koyama, R. & Ikegaya, Y. Mossy fiber sprouting as a potential therapeutic target for epilepsy. *Curr. Neurovasc. Res.* **1**, 3–10 (2004).
43. Weiler, I.J. *et al.* Fragile X mental retardation protein is translated near synapses in response to neurotransmitter activation. *Proc. Natl. Acad. Sci. USA* **94**, 5395–5400 (1997).
44. Edbauer, D. *et al.* Regulation of synaptic structure and function by FMRP-associated microRNAs miR-125b and miR-132. *Neuron* **65**, 373–384 (2010).
45. Xu, X.L., Li, Y., Wang, F. & Gao, F.B. The steady-state level of the nervous system–specific microRNA-124a is regulated by dFMR1 in *Drosophila*. *J. Neurosci.* **28**, 11883–11889 (2008).
46. Siegel, G. *et al.* A functional screen implicates microRNA-138-dependent regulation of the depalmitoylation enzyme APT1 in dendritic spine morphogenesis. *Nat. Cell Biol.* **11**, 705–716 (2009).

ONLINE METHODS

Animal care. All procedures conformed to the ARVO Statement for the Use of Animals in Ophthalmic and Vision Research and were approved by the Institutional Safety Committee on Recombinant DNA Experiments and the Animal Research Committee of Osaka Bioscience Institute. Mice were housed in a temperature-controlled room at 22 °C with a 12 h light/dark cycle. Fresh water and rodent diet were available at all times.

Generation of *Rncr3*$^{-/-}$ mice. We obtained *Rncr3* genomic clones from a screen of the 129/SvEv mouse genomic DNA library (Stratagene). We subcloned a 6.5-kb SalI-EcoRI fragment and a 4.4-kb SalI-SalI fragment from *Rncr3* genomic clones into a modified *pPNT* vector, and transfected the linearized targeting construct into the TC1 embryonic stem cell line. Genomic DNA from the liver was digested with BamHI or EcoRV, and hybridized with 5′ and 3′ probes, respectively.

Northern blot analysis. Northern blot analysis was performed as described previously[47]. An approximately 2.2-kb fragment (the BglII-BglII fragment) of mouse *Rncr3* cDNA (GenBank #BC096449) was used to synthesize the DNA probe.

PAGE northern for miR-124a. Total RNAs from mouse tissues were isolated by Trizol (Invitrogen). We denatured 20 μm of total RNAs in 5 mM EDTA containing formamide at 80 °C for 5 min, then separated them on 15% denaturing (7 M urea) polyacrylamide gels. RNAs were transferred to a nylon membrane (Pall Corporation Biodyne) at a constant current (3.3 mA cm^{-2}) for 35 min. The filter was baked for 1 h at 80 °C. LNA-modified anti–miR-124a (EXIQON, 20 pmol) was end-labeled with γ-^{32}P-ATP (3,000 Ci mmol^{-1}, Muromachi Yakuhin) using T4 polynucleotide kinase (Takara) and purified on spin columns (GE Healthcare Micro SpinTM G-25). The nylon filters were hybridized with the labeled probe in salmon sperm–containing hybridization solution (120 mM sodium phosphate (pH 7.2), 250 mM sodium chloride, 7% SDS (wt/vol) and 50% formamide (vol/vol) at 43 °C overnight, and washed twice with 0.1% SDS containing 2× SSC at 25 °C for 5 min. The filters were then exposed to X-ray film.

***In situ* hybridization.** *In situ* hybridization was performed as described previously[47]. Digoxigenin-labeled riboprobes were synthesized by T7, SP6, or T3 RNA polymerase using the *Rncr3* (same as the 3′ probe region in northern blots), *pri-miR-124a-2* (**Supplementary Table 1**), *Lhx2* (ref. 48, **Supplementary Table 1**), *Ngn2* (an EcoRI-*Xba*I fragment of cDNA AK143190), *Crx* or *Otx2* (ref. 19) cDNA as a template in the presence of 11-digoxigenin UTPs (Roche). For miR-124a detection, we used anti–miR-124a modified with a digoxigenin-labeled LNA probe (EXIQON).

Immunostaining. For immunohistochemistry, 14-μm retina and brain sections were washed twice in phosphate-buffered saline (PBS), and permeabilized with 0.1% Triton X-100 (wt/vol) in PBS, then incubated with PBS containing 4% donkey serum (vol/vol) for 1 h to block samples. The samples were incubated with a primary antibody (**Supplementary Table 2**) at 4 °C overnight. After PBS-washing, these samples were incubated with secondary antibodies at 25 °C for 1 h.

For whole-mount immunostaining of the retina, each retina was gently peeled off from the sclera, rinsed in PBS and fixed with 4% paraformaldehyde (wt/vol) in PBS for 2 h. The retinas were permeabilized by incubation in 0.1% Triton X-100 in PBS for 30 min. After washing in PBS, samples were blocked with 4% donkey serum and 0.02% Triton X-100 in PBS for 3 h. The retinas were then immunostained with primary antibodies to M-opsin and S-opsin (**Supplementary Table 2**) at 4 °C overnight. Reactions with secondary antibodies were performed overnight at 4 °C.

Western blot analysis. Western blot analysis was performed as described previously[47]. The membrane was incubated with mouse antibody to Flag (1:5,000, Sigma) or goat antibody to LHX2 (3:500; Abcam). The membrane was then incubated with a horseradish peroxidase–conjugated donkey antibody to mouse IgG (1:10,000, Jackson) or rabbit antibody to goat IgG (1:10,000, Zymed). For secondary immunoreaction, the PVDF membrane was incubated with WB Stripping Solution (Nacalai Tesque) to remove antibodies, and blocked again with 5% skim milk (wt/vol) in TBS. Further immunoblots were performed using rat antibody to GFP (1:2,000, Nacalai Tesque) or mouse antibody to β-actin (ACTB, 1:5,000, Sigma). The signals were measured using ImageJ (US National Institutes of Health).

ERG. Electroretinographic recordings were performed as described in detail[47]. In brief, ERGs were picked-up with a gold-wire loop electrode placed on the cornea. The mice were placed in a Ganzfeld bowl and stimulated with four levels of stroboscopic stimuli ranging from −5.0 to 1.0 log cd s m^{-2} to elicit scotopic ERGs, and four levels of stimuli ranging from −0.5 to 1.0 log cd s m^{-2} for the photopic ERGs. The photopic ERGs were recorded on a rod-suppressing white background of 1.3 log cd m^{-2}.

Plasmid constructs. The *Lhx2* cDNA fragment was amplified by PCR (**Supplementary Table 1**) using PrimeStar (Takara), and cloned into the *pGEM-TEasy* vector (Promega). *Lhx2* 3′ UTR–containing fragments were also amplified and cloned into *pGEM-TEasy*. Mutations in the seed match region were introduced by PCR primers (**Supplementary Table 1**). The fragments of *Lhx2* cDNA and *Lhx2* 3′ UTR were ligated into the *pCAGGS* vector. To perform the luciferase assay, we constructed a miR-124a expression plasmid. Pre-miR-124-1, pre-miR-124-2 and pre-miR-124-3 were amplified by PCR (**Supplementary Table 1**) using ExTaq polymerase (Takara), and each PCR-amplified fragment was cloned into *pCRII* plasmids (Invitrogen). After verifying the sequence, we subcloned them into *pBAsi-mU6* (Takara). The *Lhx2* 3′ UTR were ligated into *pmirGLO* (Promega) to generate *pmirGLO–Lhx2-Nat* and *pmirGLO–Lhx2-Mut*. For *Lhx2* knockdown, *pBAsi-mU6* was used for DNA vector–based shRNA synthesis. Three target sequences, shLhx2-1, shLhx2-2 and shLhx2-3 (**Supplementary Table 1**), were selected from different positions in the mouse *Lhx2* open reading frame and subcloned into the *pBAsi-mU6* vector. The inhibition abilities of shLhx2-1, shLhx2-2 and shLhx2-3 were tested by western blot analysis using cultured cells (**Supplementary Fig. 11a,b**). The strongest inhibitor of Lhx2, shLhx2-3, was used.

Generation of miR-124a-2 transgenic mice. The *pCrx2k-Cre* plasmid[19] was digested with XhoI and BamHI to remove the *Cre* gene (*pCrx2k*). *RIP-miR-124a-2* (a gift from T. Maniatis, Harvard University)[5] is a pre-miR-124a-2 expression vector that encodes pre-miR-124a-2 in an intron of the *Ds-Red* gene. We digested *RIP-miR-124a-2* and ligated it into the *pCrx2k* plasmid (*pCrx2k-Ds-Red-124a-2*; **Supplementary Fig. 9a**). To construct a transgene vector of miR-124a-2 to rescue the hippocampal phenotype, we ligated the *pUC18-4.3Syn-CAT* plasmid (a gift from M. Kilimann, Ruhr-Universität Bochum)[26] containing a rat 4.3-kb *Syn1* promoter into Ds-red-124a-2 (*pSynI4.3k-Ds-Red-124a-2*; **Supplementary Fig. 10a**). The purified construct was injected into the pronuclei of fertilized one-cell eggs of B6C3F1 mice (Oriental Bio Service) followed by implantation into pseudopregnant foster mothers (ICR mice, Japan SLC).

Luciferase assay. We transfected 0.5 μg of the reporter plasmid DNA (*pmirGLO*, *pmirGLO–Lhx2-3′ UTR-Nat* or *pmirGLO–Lhx2-3′ UTR-Mut*) and 2 μg of miR-124a expression vector DNA (*pBAsi-mU6*, *pBAsi-mU6–pre-miR-124a-1*, *pBAsi-mU6–pre-miR-124a-2* or *pBAsi-mU6–pre-miR-124a-3*) per well into HEK 293T cells in a 6-well plate using the calcium phosphate method. After transfection, the cells were incubated for 48 h and lysed with Reporter Lysis Buffer (Promega). P0 hippocampal cells (approximately 2 × 10^5) were transfected with *pmirGLO–Lhx2-3′ UTR-Nat*, or *pBAsi-mU6–pre-miR-124a-1-Mut* (250 ng each) by electroporation (Amaxa Nucleofector). After transfection, the cells were incubated for 72 h, washed with PBS, and lysed with Reporter Lysis Buffer. The lysates were used for luciferase assays. Luciferase activity was measured with the Dual-Glo Luciferase Assay System (Promega) according to the manufacturer's protocol using a Wallac 1420 Multilabel Counter (Wallac). Firefly luciferase activities were determined by three independent transfections and normalized by comparison with the Renilla luciferase activities of the internal control.

***In vivo* electroporation.** *In vivo* electroporation was performed on the P0 mouse retina as described previously[47]. The *pCAGGS*, *pCAGGS–Lhx2-Nat* or *pCAGGS–Lhx2-Mut* vectors were co-electroporated with the *pCAGGS-EGFP* vector. We used *pCAGGS* vector concentrations of 0, 2 and 3 μg μl^{-1}, *pCAGGS-Lhx2* (native or mutated) concentrations of 4, 2 and 1 μg μl^{-1}, and a *pCAGGS-EGFP* concentration of 1 μg μl^{-1} to make a 5 μg μl^{-1} DNA solution mix. The electroporated retinas were harvested at P4.

TUNEL assay. Fresh frozen retinas were sectioned to a thickness of 14 μm and fixed with 4% paraformaldehyde in PBS for 1 min. The TUNEL assay was performed according to the manufacturer's protocols.

RT-PCR and qPCR analysis. Total RNA was extracted Trizol reagent (Invitrogen), and reverse transcribed into cDNA using SuperScript II reverse transcriptase (Invitrogen) with random hexamers. Quantitative PCR was performed using a SYBR GreenER qPCR SuperMix Universal (Invitrogen). Nucleotide sequences of primers are shown in **Supplementary Table 1**. To detect mature miR-124a, we isolated total RNA using the miRNeasy Mini Kit (Qiagen), and reverse transcribed using the miScript Reverse Transcription Kit (Qiagen). Real-time qRT-PCR was performed using the miScript SYBR Green PCR kit with miScript Universal primer and the miScript Primer assay (Qiagen). For the pri-miR-124a expression assay, total RNA isolated using the miRNeasy Mini Kit was reverse transcribed to cDNA using the TaqMan reverse transcription reagent kit and following the manufacturer's protocol (Applied Biosystems). Real-time qRT-PCR was performed using TaqMan Universal PCR Master Mix and specific TaqMan Pri-miRNA Assays for *Mus musculus* miR-124-1, miR-124-2 and miR-124-3 (Applied Biosystems).

Behavior test. *Rncr3*$^{-/-}$ and wild-type mice (4–5 months old) were suspended by their tails for 3 min, and clasping duration time was measured.

Timm staining and Nissl staining. Coronal sections, 14 μm thick, from P10 frozen mouse brains were stained by the neo-Timm's method[49]. After washing in de-ionized water, sections were counterstained by 0.1%(w/v) cresyl violet (wt/vol) for 5 min, washed in 100% ethanol, and incubated in xylene. Slides were coverslipped with Permount (Fisher Scientific).

Axon outgrowth assay. Neurons from P0 mouse hippocampus were dissociated using Nerve Cell Dissociation Medium (SUMILON) according to the manufacturer's protocol. The hippocampal cells (the approximate numbers are 4×10^5) were transfected with *pCAGGS*, *pCAGGS–Lhx2-Nat* or *pCAGGS–Lhx2-Mut* (250 ng each) together with the transfected cell marker plasmid, 125 ng of *pCAGGS-FGFP* by electroporation (Amaxa Nucleofector). Then, cells were cultured on 3.5-cm poly-D-lysine–coated dishes in Nerve-Cell Culture Medium (SUMILON). For Lhx2 knockdown experiments, hippocampal cells (the approximate numbers are 2×10^5) were transfected with *pBAsi-shControl*[50] or *pBAsi–shLhx2-3* (250 ng each), together with a transfected cell marker plasmid, *pCAGGS-FGFP*. At 72 h, the cells were fixed with 4% paraformaldehyde, 4% sucrose (wt/vol), and 0.02% Triton X-100 in PBS for 30 min, then washed with PBS. After blocking with 4% donkey serum in PBS, cells were incubated with primary antibodies to PROX1 and EGFP (**Supplementary Table 2**). Following PBS washes, Alexa 488–conjugated antibody to rat IgG and Cy3-conjugated antibody to rabbit IgG were used as secondary antibodies. Images of these cells were obtained using a confocal microscope LSM700 (Zeiss), and PROX1-positive axons (longest neurite) were measured using the LSM image browser (Zeiss).

Hippocampal slice culture. A P6 SD rat brain was dissected and sliced (300 μm thick). The hippocampal slices were placed onto membranes of Millicell-CM culture inserts (Millipore) and infected with *Camk2a* promoter–driven *Lhx2-IRES-mCherry* or *mock (control)-IRES-mCherry* expression lentivirus (approximately 10^{10} PFU ml^{-1} titer) into three loci of the dentate molecular layer using a micromanipulator. Nutrition medium was composed of 25% heat-inactivated horse serum, 25% Hank's balanced salt solution, and 50% MEM. The medium was changed every 2 d. After 5 DIV, the cultured slice was fixed with 4% paraformaldehyde, 4% sucrose and 0.02% Triton X-100 in PBS for 3 h, then permeabilized with PBS, and 0.1% Triton X-100 for 30 min. The sliced section was further immunostained.

Retinal explant culture and AAV infection. The P0 eyes were enucleated, and the choroid, sclera and cornea were removed. The eyecups (retinas with lens and vitreous) were incubated with fresh DMEM/F12 media containing AAV5 (approximately 1×10^{12} particles per ml titer), which bicistronically expresses *shControl* or *shLhx2* driven by the *U6* promoter and *mCherry* driven by the *CMV* promoter (*U6-shControl-CMV-mCherry* or *U6-shLhx2- CMV-mCherry*) for 1 h at 25 °C. The lens and vitreous were removed, and the retinas were explanted with the photoreceptor side up. After a 30-min incubation, 5 μl of AAV5 vector (approximately 1×10^{12} particles) was dropped to cover the surface of the explants. The explants cultured for 5 d were immunostained with an antibody to S-opsin.

Statistical analysis. Statistical comparison of datasets were performed with Student's *t*-test. For multiple comparison, we performed one-way ANOVA with Tukey-Kramer test or Kruskal-Wallis non-parametric ANOVA with Steel-Dwass multiple comparison test. Complete statistical information is described in the **Supplementary Statistical Analysis**.

47. Sanuki, R., Omori, Y., Koike, C., Sato, S. & Furukawa, T. Panky, a novel photoreceptor-specific ankyrin repeat protein, is a transcriptional cofactor that suppresses CRX-regulated photoreceptor genes. *FEBS Lett.* **584**, 753–758 (2010).
48. Gray, P.A. *et al.* Mouse brain organization revealed through direct genome-scale TF expression analysis. *Science* **306**, 2255–2257 (2004).
49. Babb, T.L., Kupfer, W.R., Pretorius, J.K., Crandall, P.H. & Levesque, M.F. Synaptic reorganization by mossy fibers in human epileptic fascia dentata. *Neuroscience* **42**, 351–363 (1991).
50. Onishi, A. *et al.* Pias3-dependent SUMOylation directs rod photoreceptor development. *Neuron* **61**, 234–246 (2009).

doi:10.1038/nn.2897

CHANGES IN AREAS OF CAPILLARY NONPERFUSION AFTER INTRAVITREAL INJECTION OF BEVACIZUMAB IN EYES WITH BRANCH RETINAL VEIN OCCLUSION

TAKAYUKI TERUI, MD,* MINEO KONDO, MD, PHD,* TADASU SUGITA, MD, PHD,* YASUKI ITO, MD, PHD,* NAGAKO KONDO, MD, PHD,† ICHIRO OTA, MD, PHD,† KENSAKU MIYAKE, MD, PHD,† HIROKO TERASAKI, MD, PHD*

Purpose: To study the effect of an intravitreal bevacizumab (IVB) on the retinal ischemia in eyes with a branch retinal vein occlusion.

Methods: Fluorescein angiography was performed before and 1 month after the IVB (1.25 mg/0.05 mL) in 58 consecutive eyes of 58 patients with macular edema secondary to a branch retinal vein occlusion. The area of capillary nonperfusion was measured on an early-phase fluorescein angiography image by an area measurement program, and the area was expressed relative to the optic disk area (DA). A blockage of the fluorescence by the retinal hemorrhage was distinguished from nonperfusion by comparisons with retinal photographs.

Results: Thirty-seven of 58 eyes did not have any capillary nonperfusion before the IVB, and capillary nonperfusion developed in 3 of these 37 eyes 1 month after the IVB. The area of nonperfusion in these 3 eyes was 0.13, 0.47, and 0.60 DA. Twenty-one of the 58 eyes had capillary nonperfusion before the IVB, and the mean (±SD) area of nonperfusion was 3.45 ± 4.66 DA before the IVB and 3.45 ± 5.19 DA 1 month after the IVB. This change was not significant ($P = 0.36$). An increase in the area of capillary nonperfusion of >1.0 DA after the IVB was seen in only 1 of all 58 eyes.

Conclusion: These results suggest that the incidence of a significant increase in the area of capillary nonperfusion (>1 DA) during the 1 month after the IVB is very low in eyes with branch retinal vein occlusion.

RETINA 31:1068–1074, 2011

Vascular endothelial growth factor (VEGF) is one of the most important molecules in the pathogenesis of abnormal vessel permeability and growth in the eye.[1–8] Increased VEGF levels have been reported in eyes with various retinal diseases, including diabetic retinopathy,[9–11] retinopathy of prematurity,[12–14] retinal vein occlusion,[15–17] and exudative age-related macular degeneration.[18,19] Recently, several anti-VEGF agents have become available for intraocular use, and the use of these agents has revolutionized the treatment of these retinal diseases.[20,21] Of all these intravitreal anti-VEGF agents, bevacizumab (Avastin, Roche Pharma, Reinach, Switzerland), a full-length humanized monoclonal antibody of VEGF, is one of the most widely used drugs.

Although clinical trials and case reports have proven the clinical usefulness of intravitreal anti-VEGF agents in various retinal diseases,[22–27] there are several unsolved issues. One of the major controversies is whether this treatment would increase retinal ischemia

From the *Department of Ophthalmology, Nagoya University Graduate School of Medicine, Nagoya, Japan; and †Miyake Eye Hospital, Nagoya, Japan.

Supported by grants-in aid 18591913 (to M.K.), 19500416 (to Y.I.), and 18390466 (to H.T.) from the Ministry of Education, Culture, Sports, Science, and Technology, Japan.

The authors have no proprietary or conflicts of interest to disclose.

Reprint requests: Mineo Kondo, MD, PhD, Department of Ophthalmology, Nagoya University Graduate School of Medicine, 65 Tsuruma-cho, Showa-ku, Nagoya 466-8550, Japan; e-mail: kondomi@med.nagoya-u.ac.jp

because the systemic use of bevacizumab is known to increase the risk of thromboembolic events, including strokes.[28] Although there are several studies that reported that intravitreal bevacizumab (IVB) did not exacerbate retinal ischemia,[29–31] some recent clinical and experimental studies suggested that IVB may worsen ischemic changes in normal and diseased retinas.[32–37]

A search of PubMed did not extract any studies that measured the area of capillary nonperfusion before and after the IVB therapy in patients with branch retinal vein occlusion (BRVO). We hypothesized that if the IVB worsened the retinal ischemia in BRVO, then the area of capillary nonperfusion would increase within a relatively short period. Thus, the purpose of this study was to compare the area of capillary nonperfusion quantitatively before and 1 month after the IVB in eyes with macular edema secondary to BRVO.

Subjects and Methods

Subjects

To study the effect of IVB on the retinal ischemia in eyes with a BRVO, fluorescein angiography (FA) was performed before and 1 month after the IVB for all patients with BRVO who received IVB therapy at the Miyake Eye Hospital from October 2006 to November 2009. We reviewed all the FA results. The eyes that had undergone other treatments, that is, vitrectomy, laser treatments, or other drug injections, before the IVB were excluded. In the end, the FA results of 58 eyes from 58 patients were studied.

The procedures used conformed to the tenets of the Declaration of Helsinki of the World Medical Association. An informed consent had been obtained from each of the patients after they were provided sufficient information in both oral and written forms on the procedures to be used. Information on off-label use of bevacizumab was also given to all subjects.

Bevacizumab Injections

The IVB was performed in an operating room under sterile conditions. The eyes were anesthetized with 1% tetracaine eyedrops, and the fornices of the eyes were irrigated with 10% povidone–iodine. Each patient received an intravitreal injection of 1.25 mg/0.05 mL of bevacizumab using a 30-gauge needle inserted 3.5 mm from the limbus. The patient's light perception was confirmed immediately after the injection. Antibiotic drops were given for 3 days after the injection.

Fluorescein Angiography and Measurement of Capillary Nonperfusion Area

Fluorescein angiograms were recorded using a high-resolution digital fundus camera (TRC-50DX; Topcon Corporation, Tokyo, Japan) before and 1 month after the initial IVB. A series of digital images was taken after the rapid intravenous injection of 5 mL of a 10% solution of fluorescein. The fundus image subtended an angle of 60° (diameter), and the optical resolution of the digital image was 2144 ×1424 pixels for fundus photograph and 1392 ×1040 pixels for FA. One digital image in the early phase of the macular area with the fovea located at the center was used for the analyses.

Capillary nonperfusion in the peripheral retina, that is, outside the central image, was not analyzed because it was difficult to measure the exact area of peripheral nonperfusion with this system. The area of capillary nonperfusion was measured using the area measurement program of a high-resolution digital system (IMAGEnet 1024 System; Topcon Corporation; Figure 1). The area of capillary nonperfusion was defined as the area where a dropout of the retinal capillary bed was detected in the FA image.[38] A blockage of the fluorescence by the retinal hemorrhage was distinguished from the nonperfusion by comparing the FA image with retinal photographs. The measurements were performed by a retina specialist (T.T.).

Visual Acuity and Foveal Thickness

The best-corrected visual acuity was measured by a standard Japanese decimal visual acuity chart at 5 m. The decimal values were converted to the logarithm of the minimum angle of resolution (logMAR) units for statistical analyses.

The foveal thickness was determined by the optical coherence tomography (Stratus model 3000; Carl Zeiss Meditec, Dublin, CA) with software version 4.0.1. After the patients' pupils were fully dilated with 0.5% tropicamide and 0.5% phenylephrine (Mydrin-P, Santen Co, Osaka, Japan), vertical and horizontal scans of 6 mm length were imaged through the fixation point. The average foveal thickness of the vertical and horizontal scans was defined as the foveal thickness. We used this manual method to measure the foveal thickness[39,40] because it has been reported that the automatic measurement of the macular thickness often fails to identify the outer border of the neural retina.[41]

Statistical Analyses

The significance of the differences in the logMAR visual acuity, foveal thickness, and the area of capillary nonperfusion between before and 1 month

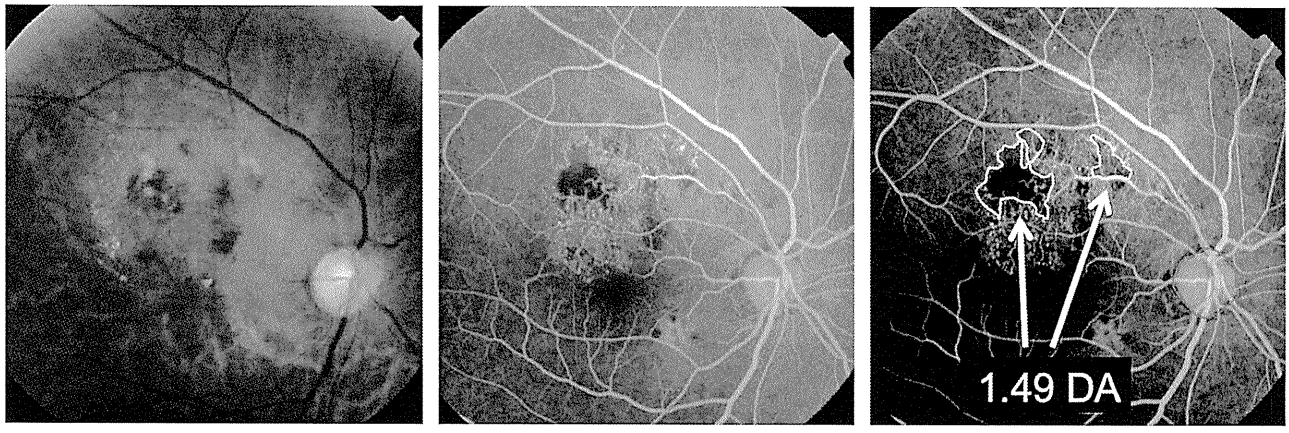

Fig. 1. Measurement of capillary nonperfusion area in a retina with BRVO. Fundus photograph (**A**) and FAs (**B** and **C**) are shown. The area of capillary nonperfusion is outlined by the use of the area measurement program of a high-resolution digital system. Blocked fluorescence lesions because of retinal hemorrhages were distinguished from nonperfusion by comparing the FA and fundus images. The area of nonperfusion is expressed relative to the DA.

after the IVB was analyzed by nonparametric Wilcoxon signed rank tests. The SPSS version 17.0J for Windows (SPSS, Inc, Chicago, IL) was used for statistical analyses. A P value of <0.05 was considered significant.

Results

Clinical Characteristics of Patients

The clinical characteristics of the 58 patients (25 men and 33 women) are summarized in Table 1. The mean age of the patients was 66.2 years (range, 41–89 years). Twenty-eight patients had systemic hypertension, 3 patients had diabetes mellitus without diabetic retinopathy, and 5 patients had hypercholesterolemia. The mean duration of the ocular symptoms before treatment was 11.0 weeks (range, 2–59 weeks).

Table 1. Baseline Clinical Characteristics of 58 Patients with Macular Edema Secondary to BRVO

Age, mean ± SD (range), years	66.2 ± 9.9 (41 to 89)
Sex	
Male/female	25/33
Period from the symptom onset to treatment, mean ± SD (range), weeks	11.0 ± 10.1 (2 to 59)
Systemic diseases	
Hypertension	28
Diabetes mellitus	3
Hypercholesterolemia	5
Visual acuity, mean ± SD (range), logMAR	0.56 ± 0.43 (−0.08 to 1.70)
Foveal thickness, mean ± SD (range), μm	565 ± 288 (155 to 1,641)

Thirty-six eyes (62.1%) had the initial IVB within 12 weeks after the onset of the symptoms.

Visual Acuity and Foveal Thickness

The mean (±SD) baseline visual acuity was 0.56 ± 0.43 logMAR units (20/69, Snellen equivalent), which significantly improved to 0.34 ± 0.37 logMAR units (20/43, Snellen equivalent) at 1 month after the IVB ($P > 0.0001$). Twenty-five of 58 eyes (43.1%) showed an improvement in visual acuity of ≥0.2 logMAR units. In contrast, only 1 eye (1.7%) showed a decrease in visual acuity of ≥0.2 logMAR units.

The mean baseline foveal thickness was 565 ± 288 μm, which significantly reduced to 256 ± 140 μm at 1 month after the treatment ($P < 0.0001$). Forty-five eyes (77.6%) showed a decrease of ≥30% in foveal thickness. Only 1 eye (1.7%) showed an increase of ≥30% in foveal thickness at 1 month after the treatment.

Changes in Area of Capillary Nonperfusion

Thirty-seven of 58 eyes did not have any capillary nonperfusion before the IVB, but new nonperfusion areas developed in 3 of these 37 eyes 1 month after the IVB. The area of nonperfusion for these 3 eyes was 0.13, 0.47, and 0.60 disk area (DA), respectively. None of these 37 eyes had an area of nonperfusion of >1.0 DA 1 month after the IVB.

Twenty-one of the 58 eyes had an area of capillary nonperfusion before the IVB, and the mean (±SD) area of nonperfusion was 3.45 ± 4.66 DA. One month after the IVB, the mean area of nonperfusion was 3.45 ± 5.19 DA. This difference was not statistically significant ($P = 0.36$). Four of these 21 eyes showed